



# Species-Specific Endotoxin Stimulus Determines Toll-Like Receptor 4- and Caspase 11-Mediated Pathway Activation Characteristics

Orna Ernst,<sup>a</sup> Mohd M. Khan,<sup>b,c\*</sup> Benjamin L. Oyler,<sup>c\*</sup> Sung Hwan Yoon,<sup>b</sup> Jing Sun,<sup>a</sup> Fang-Yu Lin,<sup>d</sup> Nathan P. Manes,<sup>b</sup> Alexander D. MacKerell, Jr.,<sup>d</sup> Iain D. C. Fraser,<sup>a</sup> Robert K. Ernst,<sup>e</sup> David R. Goodlett,<sup>e\*</sup> Aleksandra Nita-Lazar<sup>b</sup>

<sup>a</sup>Signaling Systems Section, Laboratory of Immune System Biology, National Institute of Allergy and Infectious Diseases, National Institutes of Health, Bethesda, Maryland, USA

<sup>b</sup>Functional Cellular Networks Section, Laboratory of Immune System Biology, National Institute of Allergy and Infectious Diseases, National Institutes of Health, Bethesda, Maryland, USA

<sup>c</sup>School of Medicine, University of Maryland, Baltimore, Maryland, USA

<sup>d</sup>Computer-Aided Drug Design Center, Department of Pharmaceutical Sciences, School of Pharmacy, University of Maryland, Baltimore, Maryland, USA

<sup>e</sup>Department of Microbial Pathogenesis, School of Dentistry, University of Maryland, Baltimore, Maryland, USA

Orna Ernst and Mohd M. Khan contributed equally. Author order was determined alphabetically.

**ABSTRACT** The innate immune system is the body's first line of defense against pathogens and its protection against infectious diseases. On the surface of host myeloid cells, Toll-like receptor 4 (TLR4) senses lipopolysaccharide (LPS), the major outer membrane component of Gram-negative bacteria. Intracellularly, LPS is recognized by caspase 11 through the noncanonical inflammasome to induce pyroptosis—an inflammatory form of lytic cell death. While TLR4-mediated signaling perturbations result in secretion of cytokines and chemokines that help clear infection and facilitate adaptive immunity, caspase 11-mediated pyroptosis leads to the release of damage-associated molecular patterns and inflammatory mediators. Although the core signaling events and many associated proteins in the TLR4 signaling pathway are known, the complex signaling events and protein networks within the noncanonical inflammasome pathway remain obscure. Moreover, there is mounting evidence for pathogen-specific innate immune tuning. We characterized the major LPS structures from two different pathogens, modeled their binding to the surface receptors, systematically examined macrophage inflammatory responses to these LPS molecules, and surveyed the temporal differences in global protein secretion resulting from TLR4 and caspase 11 activation in macrophages using mass spectrometry (MS)-based quantitative proteomics. This integrated strategy, spanning functional activity assays, top-down structural elucidation of endotoxins, and secretome analysis of stimulated macrophages, allowed us to identify crucial differences in TLR4- and caspase 11-mediated protein secretion in response to two Gram-negative bacterial endotoxins.

**IMPORTANCE** Macrophages and monocytes are innate immune cells playing an important role in orchestrating the initial innate immune response to bacterial infection and the tissue damage. This response is facilitated by specific receptors on the cell surface and intracellularly. One of the bacterial molecules recognized is a Gram-negative bacteria cell wall component, lipopolysaccharide (LPS). The structure of LPS differs between different species. We have characterized the innate immune responses to the LPS molecules from two bacteria, *Escherichia coli* and *Bordetella pertussis*, administered either extracellularly or intracellularly, whose structures we first determined. We observed marked differences in the temporal dynamics and amounts of proteins secreted by the innate immune cells stimulated by any of these molecules and routes. This suggests that there is specificity in the first line of response to


**Citation** Ernst O, Khan MM, Oyler BL, Yoon SH, Sun J, Lin F-Y, Manes NP, MacKerell AD, Jr, Fraser IDC, Ernst RK, Goodlett DR, Nita-Lazar A. 2021. Species-specific endotoxin stimulus determines Toll-like receptor 4- and caspase 11-mediated pathway activation characteristics. *mSystems* 6:e00306-21. <https://doi.org/10.1128/mSystems.00306-21>.

**Editor** Ileana M. Cristea, Princeton University

This is a work of the U.S. Government and is not subject to copyright protection in the United States. Foreign copyrights may apply.

Address correspondence to David R. Goodlett, [goodlett@uvic.ca](mailto:goodlett@uvic.ca), or Aleksandra Nita-Lazar, [nitalazarau@niaid.nih.gov](mailto:nitalazarau@niaid.nih.gov).

\* Present address: Mohd M. Khan, Deloitte Consulting LLP, Arlington, Virginia, USA; Benjamin L. Oyler, Tissue Analysis Core, Immunology Laboratory, Vaccine Research Center, National Institute of Allergy and Infectious Diseases, National Institutes of Health, Gaithersburg, Maryland, USA, and University of Victoria, Genome British Columbia Proteomics Centre, Victoria, British Columbia, Canada; David R. Goodlett, Department of Biochemistry and Microbiology, University of Victoria, Victoria, British Columbia, Canada, and University of Gdańsk, International Centre for Cancer Vaccine Science, Gdańsk, Poland.

 Global immunoproteomic profiling of endotoxin-stimulated macrophages uncovers specifics of TLR4- and caspase 11-mediated recognition.

**Received** 14 March 2021

**Accepted** 11 July 2021

**Published** 3 August 2021

different Gram-negative bacteria that can be explored to tailor specific therapeutic interventions.

**KEYWORDS** infection, lipopolysaccharide, Toll-like receptors, caspase 11, site identification by ligand competitive saturation, SILCS, caspases, cytokines, host response, host-pathogen interactions, inflammasome, innate immunity, macrophages, proteomics, secretome

The innate immune system responds rapidly to invading pathogens, sterile infection, and tissue damage and upregulates adaptive immunity (1). This immediate response against pathogens is facilitated by pattern recognition receptors (PRRs) that recognize pathogens' conserved molecular signatures, termed pathogen-associated molecular patterns (PAMPs) (2). To sense different microbial PAMPs, humans and mice genetically encode 11 and 13 Toll-like receptors (TLRs), respectively. On the host myeloid cells, Toll-like receptor 4 (TLR4) recognizes extracellular Gram-negative bacteria by their outer membrane component, the saccharolipid lipopolysaccharide (LPS) (3, 4), and subsequently activates the NF- $\kappa$ B and mitogen-activated protein kinase (MAPK) signaling pathways to mount the host cellular defense machinery (5, 6). Intracellularly, LPS is sensed and sampled, independently of TLR4, by caspase 4 and 5 (caspase 4/5) in humans and caspase 11 in mice via the noncanonical inflammasome machinery (7–9). Intracellular LPS induces an inflammatory form of programmed cellular death (pyroptosis) that is correlated with the maturation and secretion of the proinflammatory cytokines interleukin 1 $\alpha$  (IL-1 $\alpha$ ), IL-1 $\beta$ , and IL-18 (9, 10).

LPS is generally classified into two distinct types, "smooth LPS" and "rough LPS" (also known as lipooligosaccharide or LOS), which lacks the O-antigen moiety. Lipid A, the membrane anchor of LPS, is the minimum structural unit required for PRR recognition and activation of the host immune machinery. Lipid A structures are highly diverse between different Gram-negative bacteria, which may potentially possess a wide range of immune system agonists and antagonists that affect the host immune response (11). The number, length, and degree of unsaturation of fatty acyl chains, as well as the number of phosphate groups and their modifications, can enable, diminish, or block host immune activities (12). Mass spectrometry (MS)-based LPS structural characterization and immunoproteomics have been used to reveal how the LPS structure affects its function and to understand the molecular basis of bacterial pathogenesis (11).

Ideally, immune cells interpret the type of PAMPs they encounter and induce an appropriate inflammatory response designed to eradicate an infection without overproduction of inflammatory mediators—a threshold which, if surpassed, could potentially lead to septic shock (13). Proteins released from macrophages in response to an invading pathogen play pivotal roles in shaping immune cell communication and coordination to trigger an appropriate inflammatory response. These secreted proteins make up a subproteome, referred to as the secretome, and are released through various secretory mechanisms, including classical, nonclassical, and exosome-mediated secretory pathways, as well as membrane shedding (14–16). Recent studies of secretomes from LPS-stimulated macrophages have deepened our understanding of endotoxin recognition and function (11, 15, 17–21). The signaling events downstream from TLR4 have been studied extensively, but detailed structural and mechanistic aspects of noncanonical inflammasome-mediated LPS recognition still lack comprehensive elucidation. Identifying the secreted factors that regulate, coordinate, and propagate immune signaling is essential in order to fully decode the events specific to TLR4- and caspase 11-mediated endotoxin sensing and signaling, thus revealing the immune pathways stimulated by extracellular and/or intracellular bacteria. A better understanding of these signaling cascades is expected to facilitate rational design of vaccine adjuvants, vaccines, and immunotherapeutics against immune system dysregulation, such as for treatment of autoimmune diseases. Systems biology studies of endotoxin sensing in macrophages have been performed using transcriptomics and systems immunoproteomics approaches (reviewed in references 11 and 22). Secretome studies

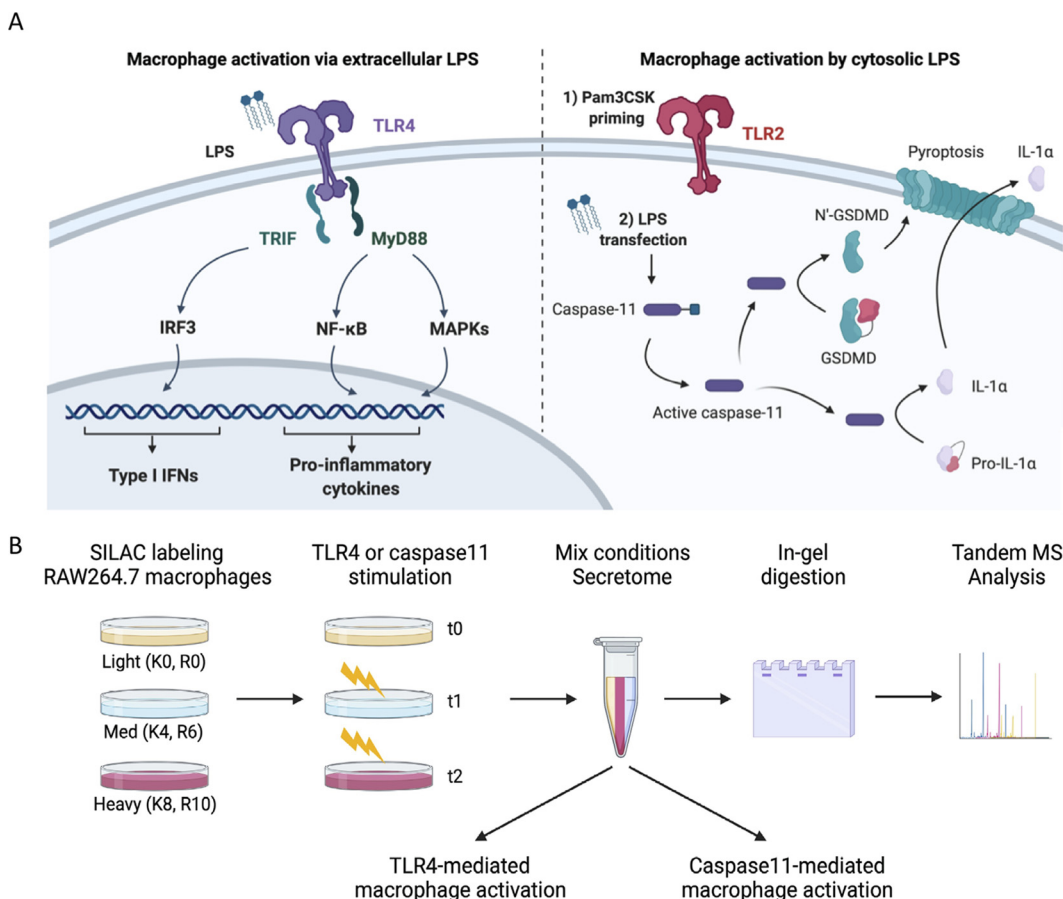


**FIG 1** Experimental design used to identify and quantify secreted proteins in response to TLR4 and noncanonical inflammasome (caspase 11)-mediated endotoxin sensing and macrophage stimulation. (A). Left, extracellular LPS activates the TLR pathway through TLR4, leading to the release of proinflammatory cytokines and type I interferons. Right, cytosolic LPS causes activation of caspase 11, resulting in noncanonical inflammasome activation. (B) Experimental design of the SILAC-labeled-secretome analysis.

provided a great deal of information about immune sensing and about the autocrine and paracrine cellular communications that shape an overall immune response to LPS (11, 15, 17, 19). MS-based strategies were used to reveal downstream substrates of the immunocaspases and their phosphorylation status (23–26). Based upon these initial proteomics data, the executor of pyroptosis, gasdermin D (GSDMD), was identified (10, 23). Nevertheless, a direct comparison between TLR4 and caspase 11 secretomes was lacking. A global systematic secretome analysis of TLR4- and caspase 11-mediated signaling could determine cellular components that orchestrate proper immune responses and elucidate the differences in the immune responses to extracellular and intracellular bacteria.

In this study, we first performed an MS-based structural characterization of the endotoxin present in two commercially available LPS extracts and then compared the macrophage responses to these two different bacterial endotoxins through TLR4- and caspase 11-mediated signaling pathways (Fig. 1). This integrative analysis resulted in an unbiased quantification and characterization of the protein secretory changes in response to extracellular versus intracellular endotoxin stimulation.

## RESULTS

**Structural profiles of *Escherichia coli* and *Bordetella pertussis* LPS.** For commercially available LPS extracts, mass spectra obtained from different vendors indicated differences in mixture composition (27). This could explain why results from biological experiments using different reagents can provide confounding results. Given that such

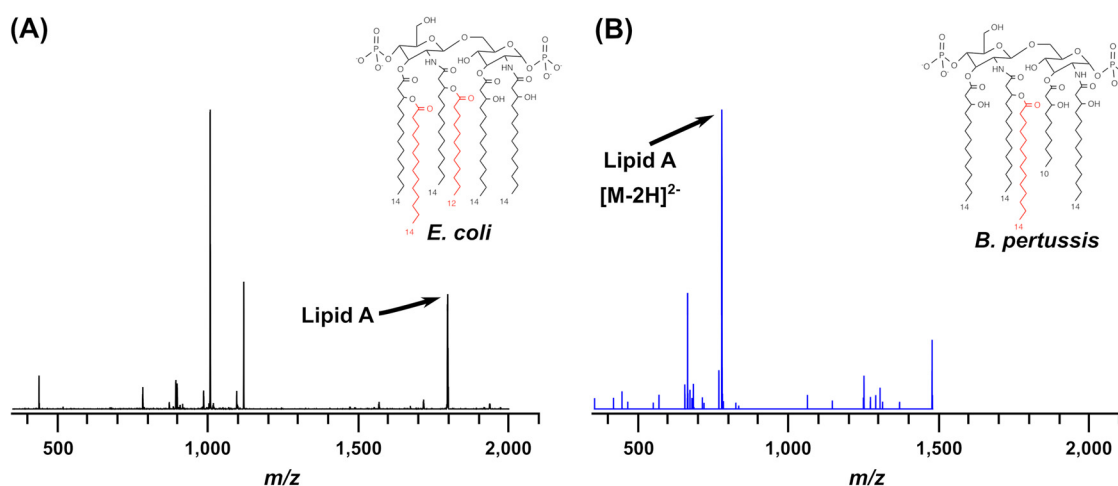


**FIG 2** Top-down MS analysis of endotoxins. MS<sup>3</sup> analysis of *E. coli*  $m/z$  1,796 (A) and *B. pertussis*  $m/z$  789 [M – 2H]<sup>2-</sup> (B) lipid A ions. MS/MS product ions from endotoxins were generated by collision-induced dissociation (CID) to confirm lipid A structural inferences as described in our recent work (27) (the data were collected across different mass ranges according to the precursor ion masses for *E. coli* J5 and *B. pertussis* 165 lipid A  $m/z$ ).

extracts are predominantly mixtures of LPS molecules, the activities of which are not individually characterized, it is difficult to know how much of a specific LPS structure is present in each mixture without characterization. It should be noted that most commercial LPS mixtures are used in biological assays without characterization of the components present in the milieu. However, it is clear that these can be different and that these extracts are functionally different. To try to avoid this uncertainty, we first characterized the LPS mixtures used in the subsequent biological experiments.

We have previously described a method to release abundant product ions corresponding to lipid A in the gas phase by analyzing intact rough-type LPS in a top-down fashion (27). The product ions for lipid A can subsequently be fragmented using collision-induced dissociation (CID) to generate MS<sup>3</sup> product ions: using gas phase decomposition, the characteristic tandem mass spectra can provide complete lipid A dissociation information and primary structural coverage that aid lipid A structure determination. Figure 2 shows MS<sup>3</sup> mass spectra for *E. coli* and *Bordetella pertussis* lipid A moieties where each produces characteristic loss of O-linked acyl chains. The MS<sup>3</sup> analysis of *E. coli*  $m/z$  1,796 and *B. pertussis*  $m/z$  789 [M – 2H]<sup>2-</sup> (–HPO<sub>3</sub>) lipid A ions confirmed that the major *E. coli* lipid A is hexa-acylated and bis-phosphorylated and that the major *B. pertussis* lipid A is penta-acylated and bis-phosphorylated.

This initial experiment will allow future data mining to explain possible experimental differences. It also allows a more direct structure-function analysis, rather than relying on LPS structures found in the scientific literature or inferred from nucleic acid data, as well as reducing the risk of error propagation. To date, there have been very few comprehensive analyses of LPS mixtures published (28–32). Doing so will allow the community to develop a database of *a priori* knowledge of LPS reagents, further making it possible to compare data from different studies, which has not been previously feasible due to a lack of quality control of LPS reagents used in experiments.

***E. coli* and *B. pertussis* LPS bind MD2-TLR4 with different affinities.** Chemical fragment cosolvent sampling techniques like the site identification by ligand competitive saturation (SILCS) method are being widely adopted to investigate ligand binding prediction in computer-aided drug design (33–35). In addition to estimating overall binding affinities in the form of ligand grid free energy (LGFE) scores, SILCS provides the binding affinity contributions of individual functional groups in lipid A. Accordingly, SILCS was used to compare the strengths of interaction of the two lipid A structures we characterized from two bacterial species with the cell surface receptor TLR4 and the coreceptor MD2 (Fig. 3). The analysis of data presented in Table 1 shows the substructure GFE (ssGFE) contributions of different fatty acid tails (3', 3'R, 2', 2'R, 3, and 2) and phosphate groups (4'P and 1-P) to

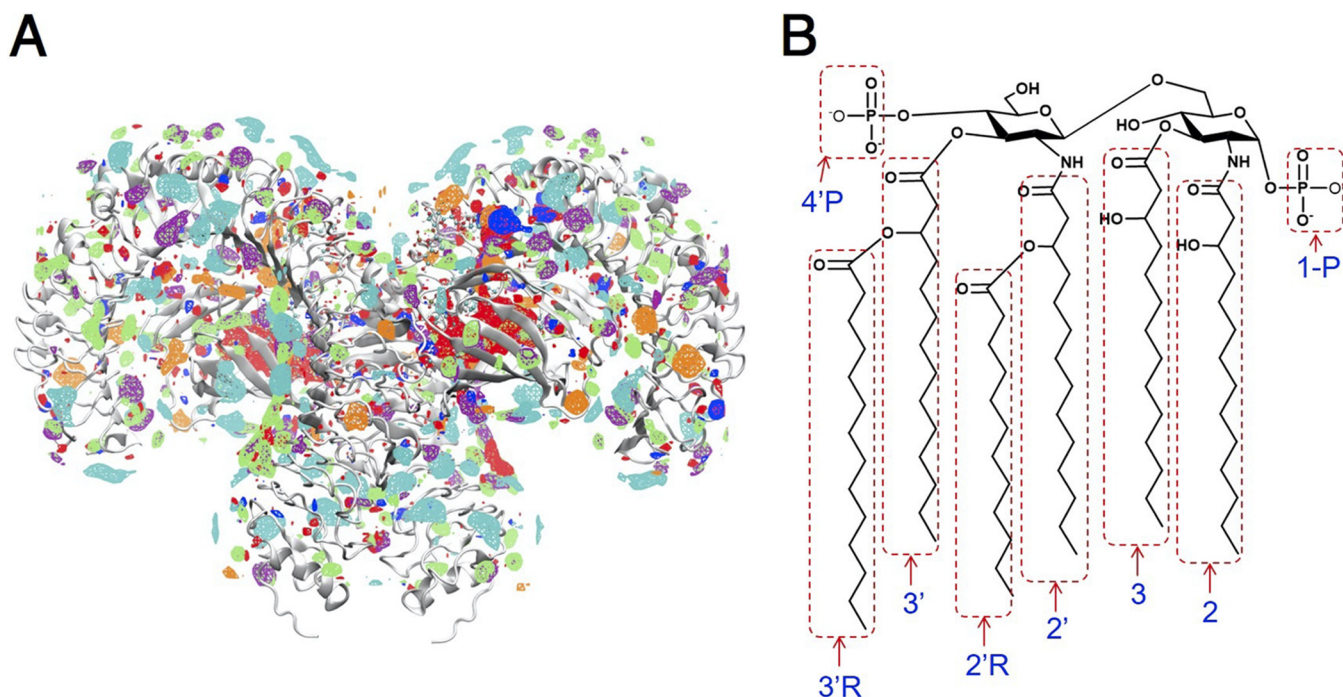


**FIG 3** (A) FragMaps obtained from the site identification by ligand competitive saturation (SILCS) simulation. FragMaps representing the functional group types as polar (green), hydrogen bond acceptor (red) and donor (blue), positive (cyan), and negative (orange) overlaid on the TLR4-MD2 crystal structure (PDB ID 3FXI) (77) shown in cartoon representation. (B) *E. coli* J5 lipid A with marked substructures. Substructures of lipid A used in the SILCS ssGFE analysis are boxed in red. Fatty acyl tails of lipid A are marked as 3', 3'R, 2', 2'R, 3, and 2, while phosphate groups are marked as 4'P and 1-P. Note that tail 3'R is not present in the *B. pertussis* 165 LPS.

the overall binding affinity, where the more negative values ( $\text{kcal mol}^{-1}$ ) of the tail moieties indicate that they make more favorable contributions than the phosphate moieties. Tail 3' makes the largest contribution to overall binding of lipid A with MD2-TLR4 receptor compared to the other moieties; additionally, 4'P makes a more favorable contribution to binding than 1-P. As suggested by the overall LGFE score, hexa-acylated bis-phosphorylated *E. coli* J5 strain lipid A interacts with MD2-TLR4 with an average LGFE score of  $-32.65 \text{ kcal/mol}$ , a stronger interaction than that of the penta-acylated bis-phosphorylated *B. pertussis* 165 strain lipid A, whose average LGFE score is  $-29.98 \text{ kcal/mol}$ . (Table 1). This more favorable binding of hexa-acylated lipid A with MD2-TLR4 may partially explain

**TABLE 1** ssGFEs and LGFEs of lipid A from *E. coli* J5 and *B. pertussis* 165 in the dimer MD2-TLR4 receptor complex, respectively

Substructure	ssGFE or LGFE ( $\text{kcal mol}^{-1}$ ) for <sup>a</sup> :					
	<i>E. coli</i> J5			<i>B. pertussis</i> 165		
	Site A	Site B	Avg	Site A	Site B	Avg
3'	-4.34	-3.85	-4.10	-4.78	-4.36	-4.57
3'R	-2.23	-2.50	-2.37	NP	NP	NP
2'	-2.89	-2.93	-2.91	-2.66	-2.99	-2.83
2'R	-2.46	-2.51	-2.49	-1.38	-2.37	-1.88
3	-2.89	-2.90	-2.90	-2.15	-3.28	-2.72
2	-2.70	-2.50	-2.60	-3.78	-3.55	-3.67
4'P	-2.62	-2.10	-2.36	-1.98	-0.94	-1.46
1-P	0.16	0.62	0.39	0.16	0.42	0.29
Sum of tails <sup>b</sup>	-17.51	-17.19	-17.35	-14.75	-16.55	-15.65
LGFE	-33.30	-32.00	-32.65	-28.75	-31.21	-29.98

<sup>a</sup>ssGFE, substructure grid free energy; LGFE, ligand GFE; NP, 3'R is not present in *B. pertussis* 165 lipid A.

<sup>b</sup>Sum of tails is the summation over the fatty acid tails 3', 3'R, 2', 2'R, 3, and 2.

why *E. coli* LPS induces stronger proinflammatory responses and more robust secretion of cytokines than the penta-acylated *B. pertussis* 165 LPS, as presented below.

***E. coli* and *B. pertussis* LPS have different immunostimulatory potentials.** Since LPS extracts are usually heterogeneous mixtures of compounds with various activities, the immune activity output is the result of the cumulative action of all LPS and other molecules present in an extract, such as ubiquitous phospholipids (27). We have compared the immunostimulatory potentials of the two commercially available LPS species extracted from *E. coli* J5 strain and *B. pertussis* 165 strain used in this study, whose dominant molecular structures we characterized (Fig. 2 and 3). While the MS data can only infer relative abundances of observed components, we observed dose- and structure-dependent tumor necrosis factor (TNF) secretion and expression for both LPS extracts in response to TLR4 stimulation. As expected, the response was species specific, or in other words, structure dependent.

The LPS extracted from *E. coli* J5 strain induced greater and faster TNF secretion in RAW264.7 cells (Fig. 4A) at all concentrations tested (Fig. 4B) and had elevated transcriptional potential in the TNF reporter THP-1 cell line (Fig. 4C) relative to LPS extracted from *B. pertussis*. These data indicate that TLR4 signaling is dependent on the endotoxin structures. In addition, we found that primary mouse bone marrow-derived macrophages (BMDM) were more responsive to the *B. pertussis* LPS (Fig. 4D) than the human TNF reporter THP-1 cell line was, although the potency of the *B. pertussis* LPS was still lower than that of *E. coli* J5 LPS. As expected, TNF secretion was not detected in response to stimulation by either LPS species when TLR4 was knocked out in *tlr4*<sup>-/-</sup> BMDM (Fig. S2A in the supplemental material), and IL-1 $\alpha$  secretion was lower (Fig. S2B).

Despite the differences observed at the transcription activation level, we found that the two major LPS species present in the mixtures used here could induce similar NF- $\kappa$ B activities at the two highest concentrations in RAW264.7 cells transfected with an NF- $\kappa$ B reporter vector (Fig. 4E). We noted that the *E. coli* J5 LPS showed greater potency, as the lower LPS concentrations induced NF- $\kappa$ B activity better than the *B. pertussis* LPS (Fig. 4E). Interestingly, the *B. pertussis* LPS did not activate type I IFN secretion at any of the concentrations tested, contrary to the dose-dependent response attained in the presence of the *E. coli* J5 LPS (Fig. 4F). Due to the lack of type I IFN measured in response to *B. pertussis* LPS, we also measured IL-6 secretion, and we found that *B. pertussis* LPS induced significantly lower levels of IL-6 than the *E. coli* J5 LPS did (Fig. 4G).

Following characterization of the TLR4-stimulatory properties of the LPS molecules present in the commercial preparations, we analyzed their noncanonical inflammasome activity potentials in response to cytosolic LPS. To do so, we applied the prime-trigger assay as follows: we first primed RAW264.7 cells or BMDM with the TLR2 agonist Pam3CSK (P3C) and then triggered the response by transfecting the cells with 100 ng ml<sup>-1</sup> of the LPS molecules for 24 h. Control (untreated) cells or those that were only primed did not secrete IL-1 $\alpha$ , whereas P3C-primed and LPS-triggered macrophages secreted IL-1 $\alpha$  after noncanonical inflammasome activation. The LPS concentration chosen for the secretome study (100 ng ml<sup>-1</sup>) stimulates macrophages sufficiently through TLR4 (Fig. 4A and B). IL-1 $\alpha$  secretion was observed in primed and triggered RAW264.7 cells (Fig. 4H) and BMDM (Fig. 4I), with *E. coli* J5 LPS eliciting a slightly stronger response in RAW264.7 macrophages. TNF was not significantly reduced (Fig. S2C), but IL-1 $\alpha$  was attenuated in the absence of caspase 11 when *Caspase1/11*<sup>-/-</sup> BMDM were primed and triggered (Fig. S2D). NLRP3 inflammasome-dependent IL-1 $\beta$  secretion can be measured only in BMDM due to insufficient expression of the ASC adaptor in RAW264.7 cells. BMDM displayed similar IL-1 $\beta$  secretion levels in response to the two LPS strains (Fig. 4J). Prime-trigger induces pyroptosis in RAW264.7 cells via the caspase 11 inflammasome, as shown both by lactate dehydrogenase (LDH) release in the pyroptosis assay (Fig. 4K) and GSDMD cleavage (Fig. S2E). These results demonstrate that the LPS from both Gram-negative bacteria can activate the TLR4 signaling pathway and the intracellular caspase 11 pathway, although with different response characteristics (intensity and dynamics).

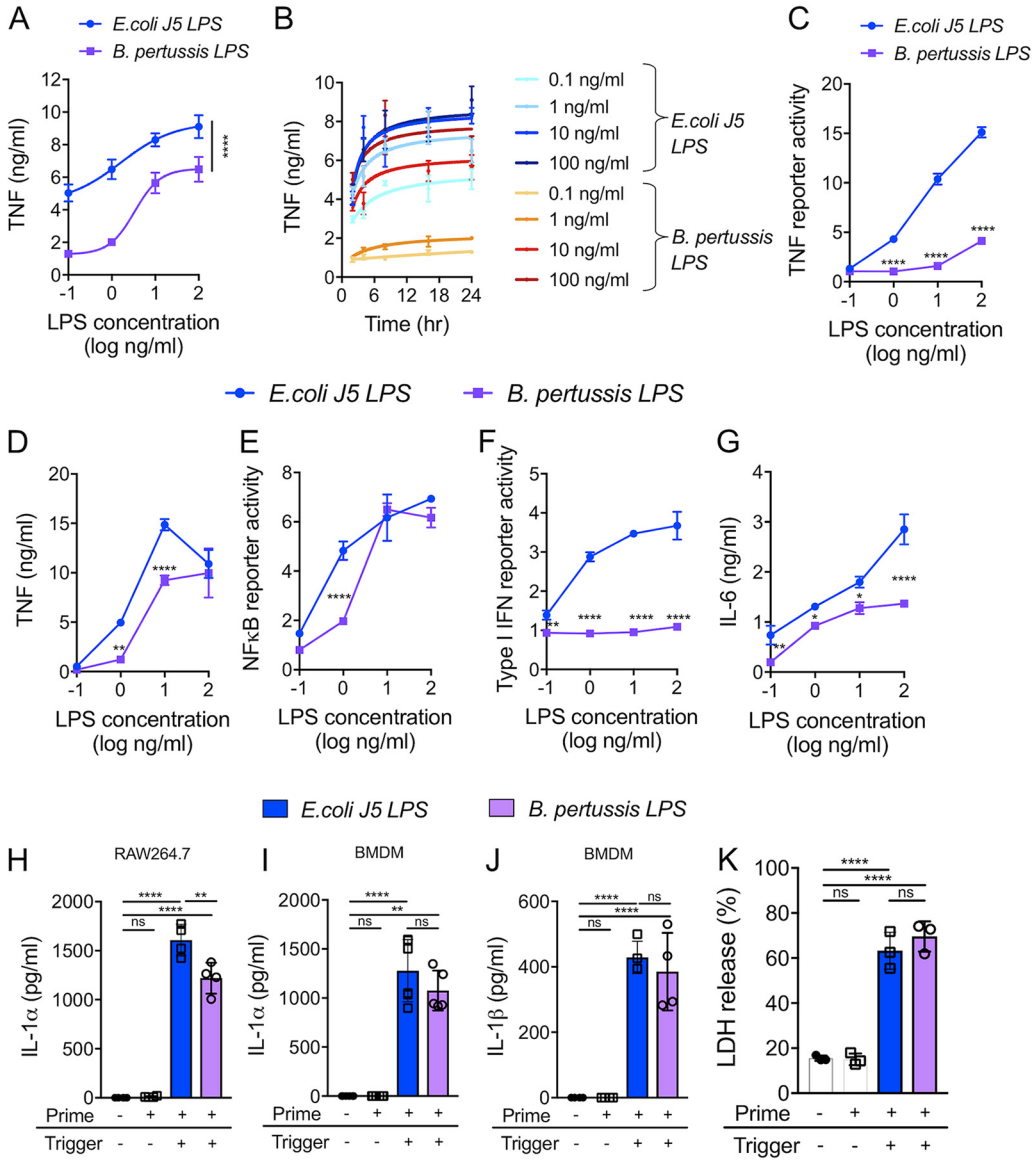


**FIG 4** TLR4- and caspase 11-mediated endotoxin recognition and macrophage stimulation. Lipid A fatty acyl variations or modifications on glucosamine phosphates determine the inflammatory potential of endotoxins in macrophages. (A, B) RAW264.7 cells were stimulated with *E. coli* or *B. pertussis* LPS at the indicated concentrations for 24 h (A) or up to 24 h (B). Secreted TNF was measured by ELISA. (C) TNF reporter THP-1 cells differentiated with phorbol myristate acetate (PMA) for 3 days were stimulated with *E. coli* or *B. pertussis* LPS at the indicated concentrations for 24 h. Luciferase reporter data were normalized against renilla luciferase activity and divided by the value for unstimulated control cells. (D) BMDM were treated with *E. coli* J5 LPS or *B. pertussis* LPS at the indicated concentrations for 24 h. Secreted TNF was measured by ELISA. (E, F) RAW264.7 cells transfected with NF-κB-luciferase reporter (E) or type I IFN reporter THP-1 cells (F) were stimulated with *E. coli* or *B. pertussis* LPS at the indicated concentrations for 24 h. Luciferase reporter data were normalized against renilla luciferase activity and divided by the values for unstimulated control cells. (G to K) RAW264.7 cells (G, H, K) and BMDM (I, J) were primed with 100 nM or 1 μg ml<sup>-1</sup> P3C (respectively) for 6 h and triggered by *E. coli* or *B. pertussis* LPS transfection for 24 h. Secreted IL-6 (G), IL-1α (H, I), and IL-1β (J) and released LDH (K) were measured by ELISA. (A to K) Data are representative of three independent experiments and expressed as mean values ± standard deviations (SD) (n=3). Statistical analysis was performed with two-way ANOVA followed by Sidak's multiple-comparison test (A to F) and one-way ANOVA followed by Tukey's multiple-comparison test (G to K). \*\*, P < 0.01; \*\*\*\*, P < 0.0001; ns, not significant.

**TLR4 and caspase 11 stimulation using *E. coli* and *B. pertussis* LPS results in distinct secretome profiles.** To investigate the global changes in protein secretion when macrophages encounter different LPS molecules extra- and intracellularly, we performed MS-based secretome analysis (Fig. 1). We first generated a data set for proteins responding to stimuli by using label-free quantitative (LFQ) proteomics of

secretome samples induced solely by LPS from the *E. coli* J5 strain after 24 h of stimulation by activating either (i) the TLR4 pathway by extracellular LPS or (ii) the caspase 11 pathway by cytosolic LPS using the prime-trigger assay. For secretome experiments, RAW264.7 macrophage cells were chosen to distinguish noncanonical inflammasome activity from the NLRP3 canonical inflammasome, as it has been shown that caspase 11 activation leads to NLRP3 inflammasome activation as well (8). Also, to induce specific protein secretion, we treated the cells with LPS (either extracellular or cytosolic) for 6 h before changing the medium to serum free for an additional 18 h, thus allowing the cells to respond normally for 6 h before removing the fetal bovine serum (FBS), a necessary step for secretome analysis. Cell death induced by the FBS removal was negligible during that time, as we demonstrated for the method previously (15), and ATP levels were assessed using the CellTiter-Glo assay to assure cell survival over the 18-h time period (Fig. S2F).

In order to normalize the prime-trigger-induced secretome to the priming-induced secretome, we additionally measured the secreted proteins following TLR2 priming alone. From this experiment, 2,506 proteins were detected, of which the relative abundance levels of 489 were changed significantly (analysis of variance [ANOVA]) (Table S4) in the LFQ data. Comparing the different stimuli, we observed 131 proteins common to LPS (TLR4) and P3C (TLR2) priming whose secretion was elevated at least 2-fold over the basal secretion (Fig. 5A). To detect those proteins whose LFQ expression levels were induced by prime-trigger alone, the values were computed by subtraction of those responding to the overarching priming and triggering with cytosolic LPS. As expected, the majority of the proteins were not shared between the cytosolic LPS and extracellular TLR-induced secretome (Fig. 5A). The top prime-trigger-specific secretome list is shown in Fig. 5B. Two of these proteins are heat shock proteins (HSPs) (10-kDa HSP [HSPE1] and 105-kDa HSP [HSPH1]), both of which are known to be secreted in response to necrotic cell death and have been previously implicated as having immunomodulatory functions in the extracellular space. While HSPs were previously defined as danger-associated molecular patterns, they are now considered to promote immune homeostasis (36). Extracellular HSPH1 has been reported to be a ligand of the scavenger receptors SREC-I and SREC-II, as it may be an antigen chaperone, and it was shown to play a role in cancer development (37–41). Extracellular HSPE1 was suggested to have anti-inflammatory functions in the immune response (42); however, the authors were not able to recapitulate this phenotype (T. Zor, Tel-Aviv University, personal communication). Figure 5C features the comparison between the prime-induced secretome and the prime-trigger-specific released proteins, highlighting the expected IL-1 $\alpha$  cytokine, as well as HSPs (HSPE1, HSPH1, and DnaJb11) and 60S ribosomal protein L38. Interestingly, in the prime-trigger-induced secretome, we detected caspase 8, which has been shown to directly cleave IL-1 $\beta$  (43, 44) and mediate cross talk between different kinds of cell death (45). V-type proton ATPase subunits D and E (Atp6v1d and Atp6v1e) were identified as well. These proteins are parts of the ATPases controlling lysosome acidification used to restrict pathogens (46, 47). The classically LPS-induced nitric oxide synthase 2 (NOS2) was also secreted as part of the protection against invading pathogens. Interestingly, the second most secreted protein specific for cytosolic LPS was the Ca<sup>2+</sup>-binding protein reticulocalbin-2, which has been suggested to have oncogenic characteristics (48) and has been shown to be elevated in type 2 diabetes (49). Additionally, the dual-specific protein phosphatase 3 (Dusp3), known to regulate TNF production intracellularly (50), was found to be secreted in response to cytosolic LPS and may function as a danger-associated molecule extracellularly.

The hierarchical clustering analysis, including the 489 proteins whose LFQ data proved statistically significant, shows differences between different types of stimulation with *E. coli* LPS that are enriched in Gene Ontology (GO) annotations (Fig. 5D, Table S5). There is a marked difference between the CASP11 treatment and the primed-only (TLR2) and LPS (TLR4) samples. For all the GO ontologies in the lower 60% of the heatmap, those proteins are lower in all ligand treatments than in untreated samples. The induced enrichments in the top 40% are the expected cytokine/inflammation response for the



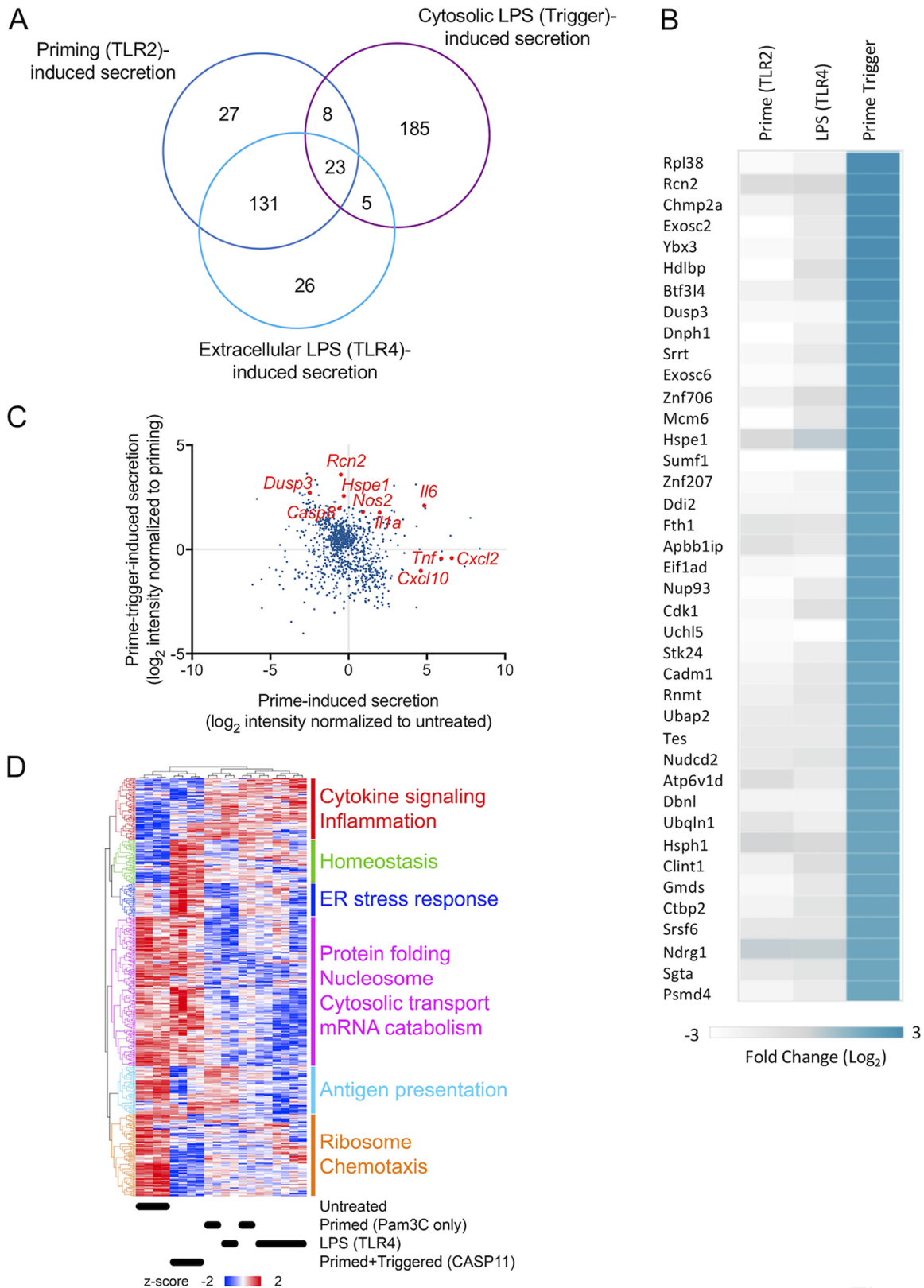


**FIG 5** Label-free TLR4- and caspase 11-mediated secretome analysis. (A) A Venn diagram representing ANOVA-significant proteins whose secretion increased at least 2-fold in response to TLR4 and TLR2 activation and compared to priming (TLR2) in the case of cytosolic LPS trigger-specific secretion. TLR4- or TLR2-induced secretion: RAW264.7 cells were treated with 100 ng ml<sup>-1</sup> *E. coli* J5 LPS or 100 nM P3C for 6 h before medium was replaced with serum-free medium for an additional 18 h. Cytosolic LPS-specific induced (Continued on next page)

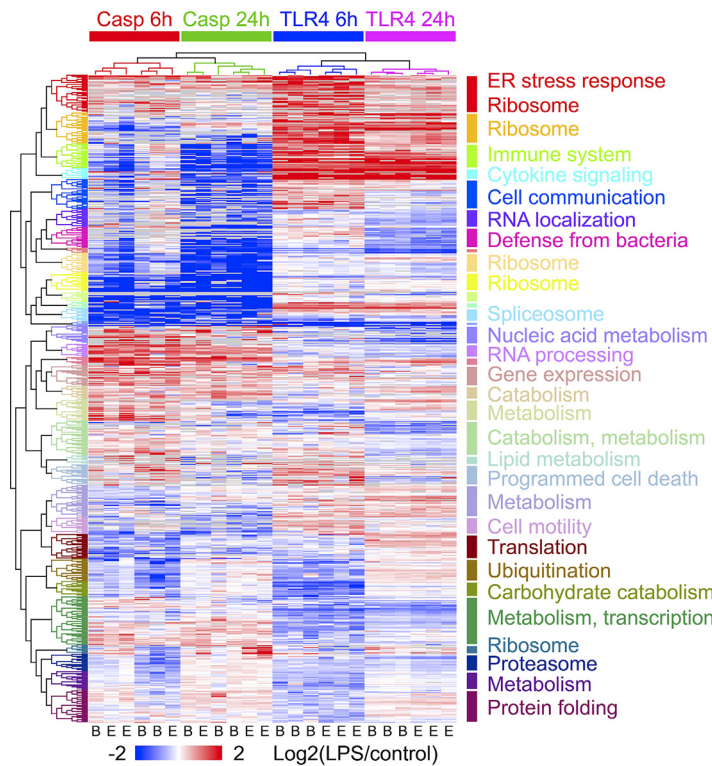


**FIG 6** Hierarchical clustering analysis of the TLR4- and caspase 11-stimulated SILAC data set. The differential expression levels of the ANOVA-significant proteins (633) are depicted (blue and red indicate down- and upregulation, respectively). The most statistically enriched GO gene annotations are depicted for each cluster. *B. pertussis* 165; *E. coli* J5.

TLR4- and TLR2-stimulated samples and cellular homeostasis and the endoplasmic reticulum (ER) stress response for the CASP11-induced inflammasome.

The LFQ analysis indicated that there are marked differences elicited by intracellular and extracellular LPS stimulations. The principal-component analysis mostly separated treated from untreated samples within principal components 1 and 2 (Fig. S3A, left) and partially separated the different treatments (Fig. S3A, right). To determine how strain-specific structural LPS differences influenced these two types of responses, we performed a comparative analysis of proteins secreted from cells stimulated by LPS from both bacterial strains, using stable isotope labeling with amino acids in cell culture (SILAC) to provide precise relative quantification. This analysis detected 2,231 proteins from all data sets obtained in biological triplicates for TLR4- and caspase 11-mediated macrophage stimulations with two different LPS molecules for 6 h and 24 h (Table S6). A total of 1,226 proteins were analyzed for their significant differential changes in expression by SILAC. Of those, 634 were found to be significant by ANOVA ( $q < 0.05$ ) (ANOVA-significant proteins) and were used for further bioinformatics analyses. The z-scored hierarchical clustering of the 634 ANOVA-significant proteins shows separation in the secretory profiles of TLR4- and caspase 11-mediated macrophage stimulations (Fig. 6, Table S5). Clusters of the ANOVA-significant proteins showing

#### FIG 5 Legend (Continued)

secretion: RAW264.7 cells were treated with 100 nM P3C for 6 h, following 100 ng ml<sup>-1</sup> *E. coli* J5 LPS transfection for 6 h, before medium was replaced with serum-free medium for an additional 18 h. (B) Heat map highlighting the top trigger-specific proteins secreted in response to cytosolic LPS. (C) Scatterplot comparing trigger-specific induced secretome and priming-induced secretome, highlighting proteins of interest discussed in the text. Quadrant labels: bottom right, priming-induced secretion; top left, prime-trigger-induced secretion; top right, priming- and prime-trigger-induced secretion; bottom left, downregulated secretion compared to control/UT. (D) HCA of the 489 ANOVA-significant proteins of the LFQ data set. The most statistically enriched GO gene annotations within each cluster are depicted. Black bars at the bottom indicate the treatment groups. From top: untreated; primed with P3C (TLR2 response); LPS stimulated (TLR4 response); primed and triggered (CASP11 response).

**TABLE 2** Selected immune system-related proteins secreted upon TLR4- and caspase 11-mediated stimulation

Protein	Gene	Fold change in:							
		TLR4 set				Caspase 11 set			
		6 h		24 h		6 h		24 h	
		BP	EC	BP	EC	BP	EC	BP	EC
Matrix metalloproteinase 9	<i>Mmp9</i>	11.64	4.14	36.59	14.88	0.66	0.35	0.33	0.24
Leucine-rich repeat transmembrane protein FLRT2	<i>Flrt2</i>	2.82	2.29	2.84	2.60	0.80	ND	0.43	ND
Vascular endothelial growth factor receptor 1	<i>Flt1</i>	3.40	2.52	3.98	3.48	0.84	0.70	0.21	0.17
Tumor necrosis factor	<i>Tnf</i>	840.30	931.11	264.21	270.69	2.72	1.65	0.45	0.41
CD44 antigen	<i>Cd44</i>	3.28	1.60	3.03	2.69	0.55	0.46	0.39	0.27
Laminin subunit gamma-1	<i>Lamc1</i>	2.25	2.34	2.22	2.40	0.85	0.41	0.31	0.29
Semaphorin 4D	<i>Sema4d</i>	3.53	3.52	2.38	1.88	1.23	0.76	0.45	0.36
Complement C3	<i>C3</i>	1.36	2.30	4.54	5.78	0.83	0.44	0.47	0.33
Transforming growth factor beta-1	<i>Tgfb1</i>	4.22	4.12	3.83	3.36	0.36	0.45	0.29	0.28
Protein disulfide-isomerase	<i>P4hb</i>	1.66	1.92	2.46	2.15	0.60	0.44	1.44	1.04
Superoxide dismutase	<i>Sod2</i>	2.38	3.27	2.03	2.22	1.22	0.99	1.41	1.58
Granulocyte colony-stimulating factor	<i>Csf3</i>	23.20	13.23	89.66	47.25	0.57	0.37	0.44	0.37
Monocyte differentiation antigen CD14	<i>CD14</i>	1.40	1.16	2.65	2.33	0.51	0.36	0.31	0.33
C-X-C motif chemokine 2	<i>Cxcl2</i>	144.37	104.04	195.51	143.55	1.27	0.77	0.41	0.39
Neutrophil gelatinase-associated lipocalin	<i>Lcn2</i>	11.49	11.17	166.78	242.91	0.74	0.59	0.38	0.58
Integrin beta-2	<i>Itgb2</i>	2.58	2.05	2.72	2.55	0.69	0.32	0.16	0.19
Amyloid beta A4 protein	<i>App</i>	1.88	1.96	1.68	1.69	0.33	0.19	0.06	0.05
Intercellular adhesion molecule 1	<i>Icam1</i>	1.70	2.54	1.57	1.59	1.16	0.62	0.33	0.28
Serglycin	<i>Srgn</i>	5.65	4.54	10.13	6.34	0.55	0.19	0.06	0.05
Heme oxygenase 1	<i>Hmox1</i>	1.76	2.04	2.59	2.48	1.12	0.65	0.82	0.84
78 kDa glucose-regulated protein	<i>Hspa5</i>	3.02	2.73	3.85	4.34	0.53	0.27	1.15	0.85
Plasminogen activator inhibitor 1	<i>Serpine1</i>	11.53	12.00	8.02	6.04	1.27	0.71	0.79	0.93
Low-density lipoprotein receptor	<i>Ldlr</i>	3.59	3.84	4.23	3.60	0.43	0.23	0.21	0.20
60S ribosomal protein L12	<i>Rpl12</i>	2.65	2.61	1.50	1.75	0.69	0.84	0.73	0.54
C-C motif chemokine 9	<i>Ccl9</i>	4.73	4.86	2.88	2.88	0.91	0.92	0.31	0.41
Protein disulfide-isomerase A6	<i>Pdia6</i>	2.12	2.55	2.79	3.65	0.77	0.56	1.57	1.22
Ubiquitin-like protein ISG15	<i>Isg15</i>	3.12	3.91	5.56	4.73	0.42	0.41	0.91	1.05
10-kDa heat shock protein	<i>Hspe1</i>	5.31	6.02	1.87	1.54	1.87	1.58	2.31	3.79
Pleckstrin	<i>Plek</i>	1.91	4.52	3.25	3.43	1.61	0.87	1.51	1.09
Leukocyte Ig-like receptor subfamily B member 4	<i>Lilrb4</i>	3.02	2.93	1.88	1.39	0.77	0.67	0.30	0.31
Endothelial protein C receptor	<i>Procr</i>	3.86	2.44	9.77	7.58	0.45	0.22	0.33	0.40
Syndecan 4	<i>Sdc4</i>	13.22	21.38	5.23	6.00	0.58	ND	0.18	ND
Disintegrin and metalloproteinase domain-containing protein 10	<i>Adam10</i>	1.27	1.42	0.53	0.65	ND	ND	ND	ND
Disintegrin and metalloproteinase domain-containing protein 17	<i>Adam17</i>	2.24	3.11	1.16	1.37	ND	ND	ND	ND
Sialidase 1	<i>Neu1</i>	1.83	1.30	0.76	0.53	ND	ND	ND	ND
Mesencephalic astrocyte-derived neurotrophic factor	<i>Manf</i>	4.26	3.43	1.42	1.30	1.86	1.54	1.23	1.08
Cathepsin D	<i>Ctsd</i>	1.05	0.90	1.08	0.82	0.61	0.48	0.30	0.32
Cathepsin K	<i>Ctsk</i>	2.26	2.25	1.35	1.23	1.03	0.96	0.35	0.29
Cathepsin Z	<i>Ctsz</i>	1.33	1.61	1.19	0.99	0.59	0.46	0.19	0.21
Galectin 3	<i>Lgals3</i>	0.77	0.89	1.25	1.33	0.46	0.62	0.76	0.96
Lysosomal protective protein	<i>Ctsa</i>	0.99	0.90	0.84	0.65	0.61	0.36	0.21	0.20

<sup>a</sup>The fold changes are calculated SILAC quantification ratios from LPS-stimulated samples. BP, *B. pertussis* LPS-stimulated samples; EC, *E. coli* LPS-stimulated samples; ND, not detected.

expression changes indicate that TLR4 and caspase 11 mediate distinct secretion patterns within each pathway. Proteins are clustered into early and late groups of secreted proteins, indicating independent processes leading to the observed patterns of protein release. Principal-component analysis of the SILAC data showed clustering dependent on the time and type of treatment (Fig. S3B). As expected, within the top five proteins showing the strongest secretion fold changes for expression in response to TLR4 signaling, three were the cytokine and chemokines TNF, CXCL2, and CSF3 (Table 2), which aided validation of the secretome data. While the two LPS species show high correlation in the secretomes associated with TLR4 activation either at the early or late secretion phase (Fig. 7A and B), we detected several secreted proteins specific to only one LPS source (Fig. 7C).

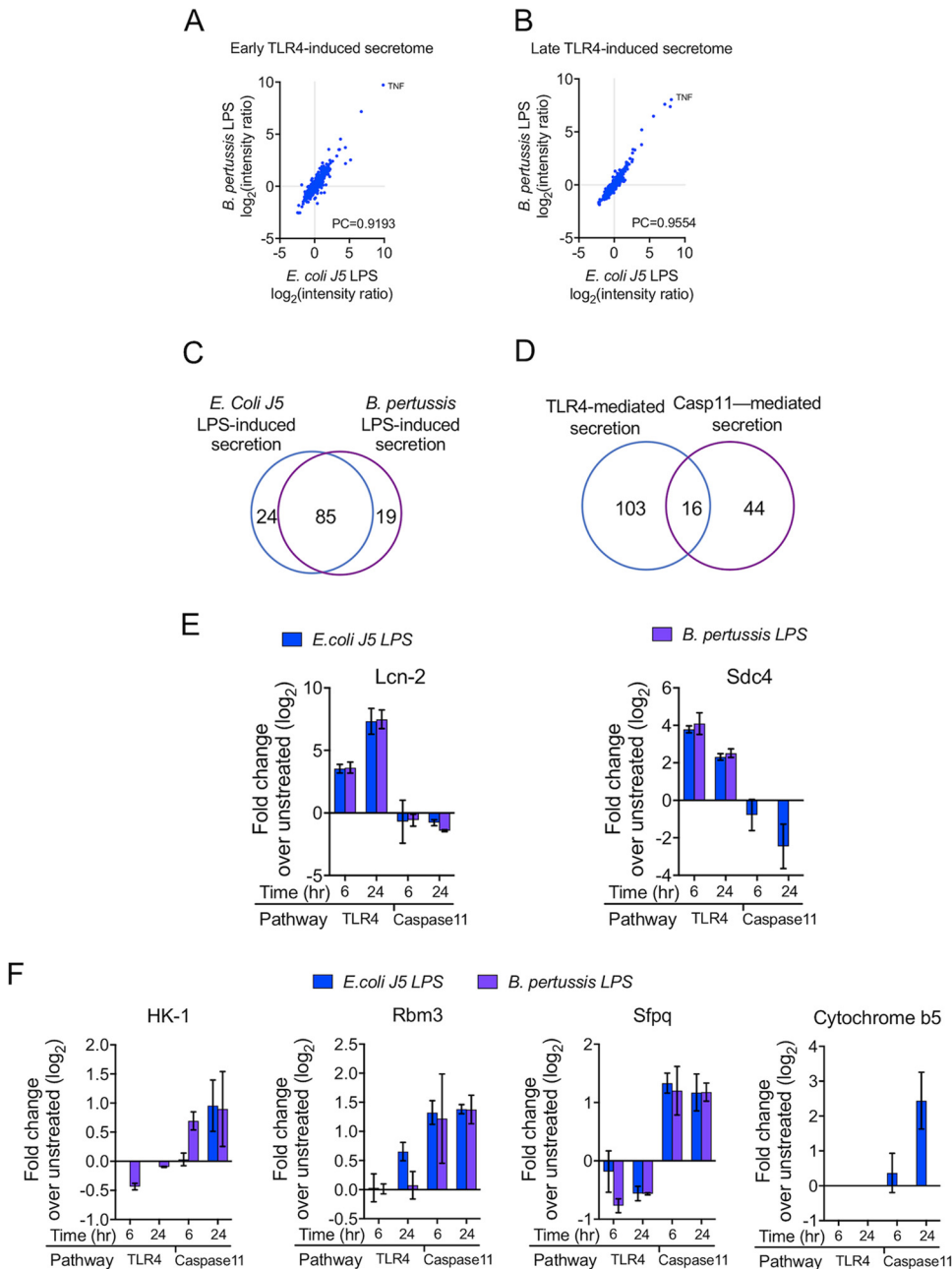


**FIG 7** SILAC-labeled comparison of the *E. coli* and *B. pertussis* LPS-induced secretomes. (A, B) Pearson correlation calculation of TLR4-mediated secretion of ANOVA-significant proteins induced by  $100 \text{ ng ml}^{-1}$  *E. coli* J5 LPS compared to *B. pertussis* 165 LPS at 6 h (A) and 24 h (B). (C) Venn diagram representing ANOVA-significant proteins whose secretion increased at least 2-fold compared to the results for untreated cells in TLR4-induced secretion after 24 h stimulation with  $100 \text{ ng ml}^{-1}$  *E. coli* J5 or *B. pertussis* 165 LPS. (D) Venn diagram representing ANOVA-significant proteins whose secretion increased at least 2-fold compared to the results for untreated cells in LPS-mediated TLR4 secretion versus prime-trigger-induced secretion at 6 and 24 h combined. (E) Analysis of Lcn-2 and Sdc4 secretion in response to  $100 \text{ ng ml}^{-1}$  *E. coli* J5 or *B. pertussis* LPS at 6 h and 24 h, normalized to the values for untreated cells. (F) Secretion levels of four selected proteins showing significant differences between TLR4- and caspase 11-activated pathways. HK-1, hexokinase 1; Rbm3, RNA binding motif protein 3; Sfpq, splicing factor proline- and glutamine-rich.

Notably, the elevated secretion profiles of the proteins associated with the TLR4 signaling pathway and the caspase 11 pathway are largely distinct (Fig. 7D). The significantly affected proteins of the LFQ and SILAC data sets were compared to each other, and roughly half of each data set was common to both data sets (Fig. S1B). Also, both of these data sets were compared to a mouse macrophage intracellular proteome data set from

our previous study (15) that identified proteins significantly affected by LPS or P3C stimulation. Only ~10% of the LFQ and SILAC data sets was also present in the intracellular proteome data set (Fig. S1B), suggesting that intracellular protein abundance changes did not significantly affect the secretome. Among the top five proteins whose secretion was elevated exclusively in response to TLR4 pathway activation by the two LPS strains were the tolerance-promoting lipocalin 2 (Lcn2) (51) and Sdc4, which has been shown to induce immune cell chemotaxis in an LPS-induced sepsis model (Fig. 7E) (52). On the other hand, pyroptosis-mediated secretion leads to pore formation on the cell membrane and to the release of proteins normally localized to the intracellular space. Highly secreted proteins induced by the caspase 11 pathway are highlighted in Fig. 7F. We observed secreted cytosolic proteins including hexokinase 1 (HK-1) and creatine kinase B, nuclear RNA binding proteins (Rbm3 and FUS) and splicing factors (Sfpq and Lsm2), and mitochondrial proteins like cytochrome *c* oxidase and cytochrome *b<sub>5</sub>* (Fig. 7F). A STRING database analysis (Fig. S4) performed using all the significantly affected proteins from both the LFQ and the SILAC data sets shows the protein-protein interactions that were affected by TLR and/or CASP11 activation in the secretome. The analysis of the secretion mechanisms summarized in Fig. S1A indicated that about half of the detected proteins were predicted to be secreted either by classical or nonclassical secretory pathways. The proteins not defined as secreted may have exited the cells through pores created as a result of the inflammatory pathway activation, organelle damage, or other mechanisms, as suggested by a recently published study by Phulphagar et al. (53).

## DISCUSSION

LPS extracts are heterogeneous mixtures of biosynthetic precursors and products that produce heterogeneous mass spectra. Activity is generally associated with a given dominant structure from such extracts, but the overall apparent biological activity of endotoxin treatment of cells is, in fact, the sum of the activities of different molecules in these mixtures that can contain an array of TLR4 complete/full agonists and antagonists. We have earlier shown the inherent heterogeneity of LPS extracts (27), and therefore, we here used two different purified Gram-negative bacterial LPS extracts, as vendor-to-vendor and species-to-species heterogeneity can be present in LPS extracts that in turn can affect the experimental results obtained from treated cells.

SILCS molecular modeling indicated that bis-phosphorylated hexa-acylated lipid A molecules, such as in *E. coli* J5 strain, bind to MD2-TLR4 more efficiently than the bis-phosphorylated penta-acylated *B. pertussis* 165 strain lipid A. The apparent favorable binding of hexa-acylated lipid A with MD2-TLR4 may partially explain why *E. coli* LPS induced stronger proinflammatory responses and more robust secretion of cytokines than the penta-acylated *B. pertussis* 165 LPS. *In vitro* macrophage activation showed endotoxin dose-, time-, and structure-dependent activities of TLR4- and caspase 11-mediated secretion. Endotoxin sensing through TLR4 and caspase 11 leads to macrophage stimulation, where stimulated cells secrete characteristic PAMP-specific proteins. TLR4 activation (by extracellular LPS, similar to when the cell encounters the Gram-negative bacteria *in vivo*) is known to induce the secretion of the inflammatory mediators cytokines and chemokines, while caspase 11 activation by cytosolic LPS leads to pyroptotic cell death and the secretion of damage-associated molecular patterns. We introduced the LPS into the cells by transfection, a method introduced by others (9), mimicking the LPS found in cytosol either from cytosolic Gram-negative bacteria, such as *Burkholderia* spp., which escape the phagosome (7), or possibly released from the endosome (the precise mechanism of LPS release into the cytosol during infection is still unclear) (54, 55). To delineate the differences between the two pathways and the two LPS structures, we used TNF- $\alpha$  secretion as a readout for TLR4 activation, whereas IL-1 $\alpha$  was specifically secreted through noncanonical inflammatory activation. As expected, we found that the LPS structure could affect the intensity of the macrophage response, as *E. coli* LPS elicited a stronger response than *B. pertussis* LPS.

Differentially secreted proteins exhibited temporal secretion differences for early (6 h) versus late (24 h) secretion for both TLR4- and caspase 11-stimulated macrophages. The

heatmap clustering visible in the LFQ data set also confirms the emerging theme for many inflammasome triggers that they induce significant cell stress, visible as the ER stress that activates the pyroptotic response, disrupting the cellular homeostasis.

Several proteins related to immune function, immunomodulation, pathogen clearance, and antimicrobial response were detected. For instance, the chemokine CXCL2 is critical and TNF secretion exacerbates inflammation; these factors were overexpressed and secreted in greater relative amounts from TLR4-stimulated cells than from the cells stimulated through caspase 11. Earlier secretome studies demonstrated that ADAM-10 and ADAM-17 secretion in LPS-stimulated macrophages correlated with overall cytokine secretion (e.g., TNF), which was secreted in caspase 11-independent fashion (56). We also detected elevated secretion of ADAM-17, MMP9, and TNF in stimulated macrophages. CSF3 induces LPS sensitization via upregulation of LPS binding protein (57) and was oversecreted in the late (24 h) phase of TLR4-stimulated cells. Cathepsins, which fine tune immune responses, are implicated in the pathogenesis of numerous diseases (58). Deficiency of Ctsk has been associated with decreased expression of TLR4, TLR5, and TLR9 and cytokine secretion (59). Like caspases, cathepsins are also involved with cell death and immune response (58). Both TLR4- and caspase 11-stimulated macrophages secreted cathepsins in response to LPS stimulation; the secretion of cathepsins in TLR4-mediated LPS-stimulated macrophages was sustained even in the latest phase (24 h). Another protein of interest, mesencephalic astrocyte-derived neurotrophic factor (MANF), a negative regulator of LPS-mediated inflammation, attenuates the inflammatory process by modulating the phosphorylation of p38 mitogen-activated protein kinases (MAPKs) and activation of the NF- $\kappa$ B pathway (60). MANF levels were higher under both conditions in the early phase (6 h) and were diminished at the latest time point (24 h). This suggests that MANF secretion is temporally regulated to fine tune LPS-mediated inflammation.

In macrophages, NF- $\kappa$ B is activated by low LPS concentrations, while MAPK pathway activation requires passing a specific threshold in LPS concentration to exhibit distinct, divergent stimulations in response to LPS (61). Additionally, the LPS concentration determines the overall caspase activation, subsequent IL-18 and IL-1 $\beta$  secretion, and stimulation of immune cells by LPS, so the dysregulation or overactivation of these processes may lead to endotoxic shock (62, 63). However, it should be noted that we have not investigated the complete immune secretome profiles for different LPS concentrations here. Our work, like most of the LPS proteomics and secretomics studies published to date, employed a final concentration of 100 ng ml<sup>-1</sup> for secretome profiling. Notably, our reporter-based assays indicated that for every type of LPS, the response is dose dependent. This highlights the importance of the signal specificity: the combination of the PAMP concentration and structure will change the time of receptor ligation, ensuring the appropriate immune response. The SILAC data clustering demonstrates that the structure of the LPS (pathogen species specificity) leads to a difference in the signaling through TLR4, but the CASP11 inflammasome signaling, very distinct from the TLR4 response, is not species specific. Our results suggest that the inflammatory response dynamics may distinguish not only between Gram-negative and Gram-positive infection (64) but also fine-tune the responses to different extracellular Gram-negative pathogens. The host component is equally important. We observed major amplitude differences between *E. coli* and *B. pertussis* LPS, especially in the human reporter cells (type I IFN and TNF reporter assays). When mouse cells were used, either cell line or primary, the dissimilarities between the two LPS species were observed mainly in the lower range of LPS concentrations. Those are probably host species specific, which reinforces the need to use a host model that would be most appropriate for the study goal; for example, basic pathway elucidation studies may be performed in the mouse model, but the direct search for therapeutics is best achieved using the human model. Future studies using primary macrophages specific to the most common site of infection (*E. coli*, gastrointestinal tract; *B. pertussis*, lung tissue) may reveal whether the trends we observed are indeed integral to the infections with these pathogens.

Secretome studies are emerging as a powerful tool facilitating both discovery (hypothesis-generating) and hypothesis-driven research in endotoxin biology. Our study,

integrating structural, reporter-based, and proteomics methods, uncouples the TLR4- and caspase 11-mediated secretion post-LPS sensing in macrophages and provides insights into the differences in the inflammatory responses to two types of Gram-negative-pathogen cell wall components.

## MATERIALS AND METHODS

**Top-down lipopolysaccharide structural analysis using multistage MS (MS/MS and MS<sup>3</sup>).** To determine the structures and validate the purity of different rough-type LPS preparations, top-down LPS structural elucidation was performed as described previously (27). Highly purified LPS of *Bordetella pertussis* 165 strain and *Escherichia coli* J5 strain were obtained from List Biological Laboratories, Inc. (Campbell, CA). LPS samples were dissolved at an approximate concentration of 20  $\mu\text{g ml}^{-1}$  in 2-propanol/water (50:50 [vol/vol]). These solutions were infused using a syringe pump at 5  $\mu\text{l min}^{-1}$  directly into a home-built nanoscale electrospray ionization (nESI) source of a linear ion trap (linear trap quadrupole; LTQ) mass spectrometer (Thermo Fisher Scientific, San Jose, CA). To increase ion transmission efficiency, the LTQ MS was modified with Pacific Northwest National Laboratory (PNNL)-style ion funnel optics prior to these experiments. The mass spectrometer was operated in the negative polarity mode with a capillary potential of  $-2.3$  kV, and tandem MS (MS/MS) experiments were performed in the ion trap with ultrapure helium as the collision gas. For top-down sequencing, MS<sup>3</sup> was carried out on LPS product ions that corresponded to lipid A and core oligosaccharides using stepped normalized collision energies. The MS data obtained were processed in Xcalibur version 3.0.63 (Thermo Fisher Scientific), and peak picking was performed using mMass version 5.5 (<http://www.mmass.org>) (65). Processed data were plotted using QtiPlot version 0.9.8.9, and figures were generated in Inkscape version 0.91 (<https://inkscape.org>).

**Cell culture and stable isotope labeling with amino acids in cell culture (SILAC).** The murine monocyte-macrophage cell line RAW264.7 (American Type Culture Collection [ATCC], Manassas, VA) was grown in Dulbecco's modified Eagle's medium (DMEM) at 37°C with 5% CO<sub>2</sub> in a humidified incubator and passaged every 2 to 3 days on sterile tissue culture-treated plates. "Culture medium" was DMEM supplemented with 10% fetal bovine serum (FBS; Gemini Bio-Products, West Sacramento, CA), 2 mM L-glutamine (Lonza, Walkersville, MD), and 20 mM HEPES buffer (Lonza, Walkersville, MD).

Stable isotope labeling with amino acids in cell culture (SILAC) of RAW264.7 cells was performed as described previously (66). Briefly, DMEM lacking L-lysine and L-arginine (Cambridge Isotope Laboratories, Tewksbury, MA) was supplemented with 0.398 mM L-arginine, 0.798 mM L-lysine (unlabeled or isotopically labeled), 2 mM glutamine, and 20 mM HEPES. For light-, medium-, and heavy-SILAC medium, DMEM lacking L-lysine and L-arginine was supplemented with light Arg/Lys (L-arginine [Arg0] and L-lysine [Lys0]), medium Arg/Lys (L-[<sup>13</sup>C<sub>6</sub>]arginine [Arg6] and L-[<sup>2</sup>D<sub>4</sub>]lysine [Lys4]), or heavy Arg/Lys (L-[<sup>13</sup>C<sub>6</sub>, <sup>15</sup>N<sub>4</sub>]arginine [Arg10] and L-[<sup>13</sup>C<sub>6</sub>, <sup>15</sup>N<sub>2</sub>]lysine [Lys8]), respectively. Cells were passaged in SILAC medium for at least five passages before stimulation.

**TLR4 and noncanonical inflammasome stimulations. (i) TLR4 stimulation.** RAW264.7 cells were treated with 100 ng ml<sup>-1</sup> LPS from *Bordetella pertussis* 165 or *Escherichia coli* J5 (List Biological Laboratories, Inc., Campbell, CA) for the times indicated in the text and figures.

**(ii) Caspase 11 stimulation.** RAW264.7 cells were primed with 100 nM Pam3CysSerLys4 (P3C; InvivoGen, San Diego, CA) and then triggered by transfecting with 100 ng ml<sup>-1</sup> LPS from *Bordetella pertussis* 165 or *Escherichia coli* J5 using TransIT-TKO transfection reagent (Mirus Bio LLC, Madison, WI) and optiMEM (Gibco, Gaithersburg, MD) for the indicated times. Similarly, BMDM were primed with 1  $\mu\text{g ml}^{-1}$  P3C and triggered by transfecting with 100 ng ml<sup>-1</sup> LPS using RNAiMax (Thermo Fisher Scientific) and optiMEM for the indicated times. Untreated (UT) cells were not treated with LPS but were otherwise handled identically to the treated cells.

**Cytokine measurement.** TNF, IL-1 $\beta$ , and IL-1 $\alpha$  secretion were measured using the mouse DuoSet enzyme-linked immunosorbent assay (ELISA) kit (R&D Systems, Minneapolis, MN) according to the manufacturer's instructions.

**Cell death and pyroptosis assays.** Cellular cytotoxicity was assayed by quantifying released lactate dehydrogenase (LDH) (67) using an LDH cytotoxicity assay kit (Pierce Biotechnology, Rockford, IL) according to the manufacturer's instructions. GSDMD cleavage was measured by Western blotting using an Abcam antibody against GSDMD (catalog number ab228005).

**Preparation of the secretome samples for liquid chromatography (LC)-MS/MS analysis.** RAW264.7 cells (light-, medium-, or heavy-SILAC labeled) were plated in 12-well dishes at  $5 \times 10^5$  cells per well and incubated overnight at 37°C in 5% CO<sub>2</sub> in a humidified incubator. Prior to LPS stimulation (i.e., prior to extracellular or cytosolic LPS stimulation), FBS-containing culture medium was removed, the cells were washed once with FBS-free culture medium, and the cells were incubated in FBS-free culture medium during the TLR4 and CASP11 stimulations.

For the extracellular LPS (i.e., TLR4) stimulations, the light-SILAC cells were untreated for 24 h, the medium-SILAC cells were untreated for 18 h and then stimulated for 6 h with 100 ng ml<sup>-1</sup> LPS, and the heavy-SILAC cells were stimulated for 24 h with 100 ng ml<sup>-1</sup> LPS (Fig. 1A, left).

For the intracellular LPS (i.e., CASP11) stimulations, the light-, medium-, and heavy-SILAC cells were primed using 100 nM P3C for 6 h. Subsequently, the primed light-SILAC cells were not treated further for 24 h, the primed medium-SILAC cells were untreated for 18 h and then transfected and incubated for 6 h with 100 ng ml<sup>-1</sup> LPS, and the primed heavy-SILAC cells were transfected and incubated for 24 h with 100 ng ml<sup>-1</sup> LPS (Fig. 1A, right).

In addition to the SILAC-labeled cells, non-SILAC-labeled cells were also used for secretomics analyses using label-free quantitative (LFQ) proteomics. TLR4 stimulation was performed by stimulating

RAW264.7 macrophages with  $100 \text{ ng ml}^{-1}$  LPS (*Escherichia coli* J5 LPS) for 6 h in culture medium, followed by washing and medium replacement with serum-free culture medium for an additional 18 h. Caspase 11 stimulation was performed by transfecting primed RAW264.7 cells with  $100 \text{ ng ml}^{-1}$  LPS for 6 h in culture medium, followed by washing and medium replacement with serum-free medium for an additional 18 h. Priming was performed by incubating RAW264.7 cells for 6 h with  $100 \text{ nM}$  P3C.

At the designated endpoints,  $450 \mu\text{l}$  of conditioned medium was removed and filtered to remove any dead cells using centrifugal filters ( $0.22\text{-}\mu\text{m}$  pore size; EMD Millipore, Tullagreen, Ireland), flash-frozen in liquid nitrogen, and stored at  $-80^\circ\text{C}$ . For the SILAC samples,  $250\text{-}\mu\text{l}$  amounts of untreated (light), 6-h-stimulated (medium), and 24-h-stimulated (heavy) samples were combined at a 1:1:1 ratio (vol/vol/vol) and then concentrated by vacuum centrifugation. Samples were then separated on one-dimensional SDS-PAGE. All LFQ and SILAC stimulations were performed in biological duplicates and triplicates, respectively (Fig. 1B).

**Sample fractionation using SDS-PAGE, in-gel trypsin digestion, and LC-MS analysis.** The secretome samples were fractionated by one-dimensional SDS-PAGE on NuPage midi 10% Bis-Tris gels (Invitrogen, Carlsbad, CA) with NuPage SDS ME5 (morpholineethanesulfonic acid) running buffer and then stained with colloidal Coomassie blue (SimplyBlue SafeStain; Life Technologies, Carlsbad, CA) (68). After destaining, each gel lane was cut into 3 (unlabeled samples) or 5 (SILAC samples) bands and the gel samples were dehydrated with acetonitrile. Dehydrated samples were reduced with  $10 \text{ mM}$  dithiothreitol in  $100 \text{ mM}$  ammonium bicarbonate for 30 min at  $56^\circ\text{C}$ . The gel samples were dehydrated with acetonitrile and then alkylated with  $55 \text{ mM}$  iodoacetamide in  $100 \text{ mM}$  ammonium bicarbonate for 20 min in the dark at room temperature. Reduced and alkylated samples were digested overnight with  $13 \text{ ng } \mu\text{l}^{-1}$  trypsin in  $10 \text{ mM}$  ammonium bicarbonate containing  $10\%$  (vol/vol) acetonitrile, as described previously (68). Peptides were extracted from the gel samples using water/acetonitrile (95:5 [vol/vol]) with  $0.1\%$  trifluoroacetic acid, followed by water/acetonitrile (40:60 [vol/vol]) with  $0.1\%$  trifluoroacetic acid. Collected solutions were dried in a vacuum centrifuge and then resuspended in  $0.1\%$  (vol/vol) formic acid,  $2\%$  acetonitrile for MS/MS analysis.

**Peptide sequencing by MS/MS, protein identification, and quantification.** All LC-MS/MS analyses were performed in data-dependent acquisition (DDA) mode using an UltiMate 3000 nanoscale LC (nanoLC) system (Thermo Fisher Scientific, Inc., Bremen, Germany) directly coupled to an LTQ Orbitrap Velos pro mass spectrometer (Thermo Fisher Scientific, Inc., Bremen, Germany) that automatically cycled between Orbitrap full-scan MS and LTQ MS/MS using a top 18 method for a 180-min linear gradient (for SILAC samples) or a top 10 method for a 100-min linear gradient (for LFQ samples). The raw mass spectrometry data were analyzed using MaxQuant version 1.6.10.43, and the Andromeda search engine was run against the mouse UniProt sequence database (downloaded December 2019) (69, 70) using the following parameters: (i) for trypsin digestion, a maximum of two missed cleavages were allowed, (ii) the maximum mass deviations for the monoisotopic precursor ions and fragment ions were set to  $6.0 \text{ ppm}$  and  $0.5 \text{ Da}$ , respectively, (iii) N-terminal acetylation and methionine oxidation were set as variable modifications, (iv) cysteine carbamidomethylation was set as a fixed modification, (v) requantification and match between runs functionalities were enabled, (vi) protein identification required at least one unique+razor peptide per protein group, (vii) the data were then filtered by setting a  $1\%$  false discovery rate (FDR) at both the peptide-spectrum-match and protein levels and protein abundance ratios were calculated for 6-h and 24-h treatments versus untreated (SILAC data set), and (viii) SILAC ratios were used to determine fold changes for the TLR4- and caspase 11-stimulated samples (68–70).

**Bioinformatic analysis and quality control.** For the LFQ analysis, the MaxQuant “LFQ intensity” values were used for the protein abundance values. The data were further filtered by requiring that at least two unique peptides were identified for each protein identification, and the protein abundance values were  $\text{Log}_2$  transformed. Missing values were imputed using Perseus version 1.6.10.0 (normal distribution, width = 0.3, downshift = 1.8) (71).

For the SILAC analysis, the data were filtered by requiring that each of the proteins was identified by at least two unique peptides. These data were further filtered by requiring that each of the proteins was successfully quantified in at least three biological replicates within at least one experimental condition. Protein abundance ratios (LPS/control) were  $\text{Log}_2$  transformed. The log-ratio values were globally normalized using the median value (i.e., “median centered”) to correct for unequal sample mixing for each time point using Perseus version 1.6.10.0 (71).

For the LFQ and SILAC data, quantified proteins were further analyzed for their differential expression and statistical significance using analysis of variance (ANOVA) tests using Perseus (a  $q$  value of  $\leq 0.05$  was required). Hierarchical clustering analyses (HCAs) were performed using Genesis version 1.8.1 (72) (z-scores were first calculated for each protein across the LFQ samples; distance = Kendall's Tau [LFQ] and Euclidean distance [SILAC]; linkage = Ward linkage). Panther version 16.0 (<http://www.pantherdb.org/>) (73) was used to perform Gene Ontology (GO) term enrichment analyses for each HCA cluster (the reference gene set was all the identified proteins; LFQ and SILAC were kept separate). The LFQ ANOVAs tested for effects resulting from the experimental condition and for batch effects. Coefficients of variation (CVs) were calculated across the biological replicates using the raw data (i.e., no log transformation, no imputation, no normalization, and no ANOVA). The CV data are included in Tables S1 and S2. Overall, the mean CVs across the biological replicates were  $26.8\%$  (LFQ data set) and  $22.8\%$  (SILAC data set). We noted that the mean CVs of the two 24-h TLR4 SILAC samples were  $10.5\%$  and  $11.2\%$ , indicating that biological variability was a major source of variance in general and that our sample preparation and LC-MS were highly reproducible. Principal-component analyses were performed using Perseus.

The secretory mechanisms were determined using SignalP 4.1 (74) and SecretomeP 2.0 (75). All of the proteins that were confidently identified in the LFQ and SILAC secretome samples were analyzed using SignalP version 5.0 (<http://www.cbs.dtu.dk/services/SignalP/>) (76) to predict proteins secreted via classical (signal peptide-mediated) secretion (Fig. S1A, Table S3). In addition, these proteins were also



analyzed using SecretomeP version 2.0 (<http://www.cbs.dtu.dk/services/SecretomeP/>) (75) to predict proteins secreted via nonclassical secretion (Fig. S1A, Table S3).

**SILCS-based molecular-modeling analysis of lipid A analog binding to the MD2/TLR4 complex.** Following previously described procedures (33), the site identification by ligand competitive saturation (SILCS) simulations were performed on the dimer structure of MD2-TLR4 (PDB ID 3FXI) (77) after removal of lipid A and solvation of the complex by water and by eight solutes that represent different chemical functionalities, including benzene, propane, acetaldehyde, methanol, formamide, imidazole, acetate, and methylammonium. From the SILCS simulations, three-dimensional (3-D) probability maps of the functional groups in the solutes, termed FragMaps, were calculated. The FragMaps are normalized based on their concentrations in aqueous solution such that they account for functional group-protein interactions, functional group and protein desolvation, and protein flexibility. The FragMaps are then converted to grid free energy (GFE) FragMaps through a Boltzmann transformation (34). The GFE FragMaps allow quantitative evaluation of the binding orientations and affinities of ligands in the binding site. To determine the binding affinities of lipid A in MD2-TLR4, lipid A structures were docked into both sites in the dimer (denoted as site A and site B) of MD2-TLR4 via the SILCS-MC (Monte Carlo) conformational sampling method based on the most favorable ligand GFE (LGFE) scores as described in previous works (34, 77, 78). The corresponding atom-based GFE scores were then summed over different substructures (i.e., contributions of different fatty acyl tails [3', 3'R, 2', 2'R, 3, and 2] and phosphate groups [4'P and 1-P]), from which the substructure GFE (ssGFE) contributions to the overall LGFE score of lipid A were obtained (Table 1).

**Data availability.** The mass spectrometry proteomics data have been deposited to the ProteomeXChange Consortium via the PRIDE (79) partner repository with the data set identifier PXD024692.

## SUPPLEMENTAL MATERIAL

Supplemental material is available online only.

**FIG S1**, TIF file, 2.4 MB.

**FIG S2**, TIF file, 2.8 MB.

**FIG S3**, TIF file, 2.8 MB.

**FIG S4**, TIF file, 2.6 MB.

**TABLE S1**, XLSX file, 0.6 MB.

**TABLE S2**, XLSX file, 0.7 MB.

**TABLE S3**, XLSX file, 0.2 MB.

**TABLE S4**, XLSX file, 0.2 MB.

**TABLE S5**, XLSX file, 1.1 MB.

**TABLE S6**, XLSX file, 0.2 MB.

## ACKNOWLEDGMENTS

This research was supported in part by the Intramural Research Program of NIH, NIAID and in part by grant number 1R01AI123820-01 from NIAID to D.R.G. and R.K.E. M.M.K. is grateful to the American Association of Pharmaceutical Scientists (AAPS) foundation for a graduate student fellowship and the Graduate Partnership Program (GPP), NIH for academic support. For funding, D.R.G. thanks the International Research Agendas Program of the Foundation for Polish Science (grant number MAB/2017/03).

The International Centre for Cancer Vaccine Science project is carried out within the International Research Agendas Program of the Foundation for Polish Science cofinanced by the European Union under the European Regional Development Fund. The University of Victoria Genome BC Proteomics Centre is grateful to Genome Canada and Genome British Columbia for financial support for Genomics Technology Platforms (GTP) funding for operations and technology development (264PRO).

A.D.M., Jr., is cofounder and CSO of SilcsBio LLC.

## REFERENCES

- Iwasaki A, Medzhitov R. 2015. Control of adaptive immunity by the innate immune system. *Nat Immunol* 16:343–353. <https://doi.org/10.1038/ni.3123>.
- Janeway CA, Jr, Medzhitov R. 2002. Innate immune recognition. *Annu Rev Immunol* 20:197–216. <https://doi.org/10.1146/annurev.immunol.20.083001.084359>.
- Medzhitov R, Preston-Hurlburt P, Janeway CA, Jr. 1997. A human homologue of the *Drosophila* Toll protein signals activation of adaptive immunity. *Nature* 388:394–397. <https://doi.org/10.1038/41131>.
- Poltorak A, He X, Smirnova I, Liu MY, Van Huffel C, Du X, Birdwell D, Alejos E, Silva M, Galanos C, Freudenberg M, Ricciardi-Castagnoli P, Layton B, Beutler B. 1998. Defective LPS signaling in C3H/HeJ and C57BL/10ScCr mice: mutations in Tlr4 gene. *Science* 282:2085–2088. <https://doi.org/10.1126/science.282.5396.2085>.
- Brubaker SW, Bonham KS, Zanoni I, Kagan JC. 2015. Innate immune pattern recognition: a cell biological perspective. *Annu Rev Immunol* 33:257–290. <https://doi.org/10.1146/annurev-immunol-032414-112240>.
- Lemaitre B, Nicolas E, Michaut L, Reichhart JM, Hoffmann JA. 1996. The dorsoventral regulatory gene cassette spatzle/Toll/cactus controls the potent antifungal response in *Drosophila* adults. *Cell* 86:973–983. [https://doi.org/10.1016/S0092-8674\(00\)80172-5](https://doi.org/10.1016/S0092-8674(00)80172-5).

7. Hagar JA, Powell DA, Aachoui Y, Ernst RK, Miao EA. 2013. Cytoplasmic LPS activates caspase-11: implications in TLR4-independent endotoxic shock. *Science* 341:1250–1253. <https://doi.org/10.1126/science.1240988>.
8. Kayagaki N, Warming S, Lamkanfi M, Vande Walle L, Louie S, Dong J, Newton K, Qu Y, Liu J, Heldens S, Zhang J, Lee WP, Roose-Girma M, Dixit VM. 2011. Non-canonical inflammasome activation targets caspase-11. *Nature* 479:117–121. <https://doi.org/10.1038/nature10558>.
9. Shi J, Zhao Y, Wang Y, Gao W, Ding J, Li P, Hu L, Shao F. 2014. Inflammatory caspases are innate immune receptors for intracellular LPS. *Nature* 514:187–192. <https://doi.org/10.1038/nature13683>.
10. He WT, Wan H, Hu L, Chen P, Wang X, Huang Z, Yang ZH, Zhong CQ, Han J. 2015. Gasdermin D is an executor of pyroptosis and required for interleukin-1 $\beta$  secretion. *Cell Res* 25:1285–1298. <https://doi.org/10.1038/cr.2015.139>.
11. Khan MM, Ernst O, Sun J, Fraser IDC, Ernst RK, Goodlett DR, Nita-Lazar A. 2018. Mass spectrometry-based structural analysis and systems immunoproteomics strategies for deciphering the host response to endotoxin. *J Mol Biol* 430:2641–2660. <https://doi.org/10.1016/j.jmb.2018.06.032>.
12. Scott AJ, Oyler BL, Goodlett DR, Ernst RK. 2017. Lipid A structural modifications in extreme conditions and identification of unique modifying enzymes to define the Toll-like receptor 4 structure-activity relationship. *Biochim Biophys Acta Mol Cell Biol Lipids* 1862:1439–1450. <https://doi.org/10.1016/j.bbalip.2017.01.004>.
13. Delano MJ, Ward PA. 2016. The immune system's role in sepsis progression, resolution, and long-term outcome. *Immunol Rev* 274:330–353. <https://doi.org/10.1111/imir.12499>.
14. Agrawal GK, Jwa NS, Lebrun MH, Job D, Rakwal R. 2010. Plant secretome: unlocking secrets of the secreted proteins. *Proteomics* 10:799–827. <https://doi.org/10.1002/pmic.200900514>.
15. Koppenol-Raab M, Sjoelund V, Manes NP, Gottschalk RA, Dutta B, Benet ZL, Fraser ID, Nita-Lazar A. 2017. Proteome and secretome analysis reveals differential post-transcriptional regulation of Toll-like receptor responses. *Mol Cell Proteomics* 16:S172–S186. <https://doi.org/10.1074/mcp.M116.064261>.
16. Makridakis M, Vlahou A. 2010. Secretome proteomics for discovery of cancer biomarkers. *J Proteomics* 73:2291–2305. <https://doi.org/10.1016/j.jprot.2010.07.001>.
17. Khan MM, Koppenol-Raab M, Kuriakose M, Manes NP, Goodlett DR, Nita-Lazar A. 2018. Host-pathogen dynamics through targeted secretome analysis of stimulated macrophages. *J Proteomics* 189:34–38. <https://doi.org/10.1016/j.jprot.2018.03.016>.
18. Manes NP, Nita-Lazar A. 2018. Application of targeted mass spectrometry in bottom-up proteomics for systems biology research. *J Proteomics* 189:75–90. <https://doi.org/10.1016/j.jprot.2018.02.008>.
19. Meissner F, Scheltema RA, Mollenkopf HJ, Mann M. 2013. Direct proteomic quantification of the secretome of activated immune cells. *Science* 340:475–478. <https://doi.org/10.1126/science.1232578>.
20. Eichelbaum K, Krijgsvelde J. 2014. Rapid temporal dynamics of transcription, protein synthesis, and secretion during macrophage activation. *Mol Cell Proteomics* 13:792–810. <https://doi.org/10.1074/mcp.M113.030916>.
21. Gillen J, Ondee T, Gurusamy D, Issara-Amphorn J, Manes NP, Yoon SH, Leelahavanichkul A, Nita-Lazar A. 2021. LPS tolerance inhibits cellular respiration and induces global changes in the macrophage secretome. *Biomolecules* 11:164. <https://doi.org/10.3390/biom11020164>.
22. Khan MM, Ernst O, Manes NP, Oyler BL, Fraser IDC, Goodlett DR, Nita-Lazar A. 2019. Multi-omics strategies uncover host-pathogen interactions. *ACS Infect Dis* 5:493–505. <https://doi.org/10.1021/acsinfecdis.9b00080>.
23. Agard NJ, Maltby D, Wells JA. 2010. Inflammatory stimuli regulate caspase substrate profiles. *Mol Cell Proteomics* 9:880–893. <https://doi.org/10.1074/mcp.M900528-MCP200>.
24. Cathelin S, Rebe C, Haddaoui L, Simioni N, Verdier F, Fontenay M, Launay S, Mayeux P, Solary P. 2006. Identification of proteins cleaved downstream of caspase activation in monocytes undergoing macrophage differentiation. *J Biol Chem* 281:17779–17788. <https://doi.org/10.1074/jbc.M600537200>.
25. Shimbo K, Hsu GW, Nguyen H, Mahrus S, Trinidad JC, Burlingame AL, Wells JA. 2012. Quantitative profiling of caspase-cleaved substrates reveals differential drug-induced and cell-type patterns in apoptosis. *Proc Natl Acad Sci U S A* 109:12432–12437. <https://doi.org/10.1073/pnas.1208616109>.
26. Turowec JP, Zukowski SA, Knight JD, Smalley DM, Graves LM, Johnson GL, Li SS, Lajoie GA, Litchfield DW. 2014. An unbiased proteomic screen reveals caspase cleavage is positively and negatively regulated by substrate phosphorylation. *Mol Cell Proteomics* 13:1184–1197. <https://doi.org/10.1074/mcp.M113.037374>.
27. Oyler BL, Khan MM, Smith DF, Harberts EM, Kilgour DPA, Ernst RK, Cross AS, Goodlett DR. 2018. Top down tandem mass spectrometric analysis of a chemically modified rough-type lipopolysaccharide vaccine candidate. *J Am Soc Mass Spectrom* 29:1221–1229. <https://doi.org/10.1007/s13361-018-1897-y>.
28. Shaffer SA, Harvey MD, Goodlett DR, Ernst RK. 2007. Structural heterogeneity and environmentally regulated remodeling of *Francisella tularensis* subspecies novicida lipid A characterized by tandem mass spectrometry. *J Am Soc Mass Spectrom* 18:1080–1092. <https://doi.org/10.1016/j.jasms.2007.03.008>.
29. Bure C, Le Senechal C, Macias L, Tokarski C, Vilain S, Brodbelt JS. 2021. Characterization of isomers of lipid A from *Pseudomonas aeruginosa* PAO1 by liquid chromatography with tandem mass spectrometry with higher-energy collisional dissociation and ultraviolet photodissociation. *Anal Chem* 93:4255–4262. <https://doi.org/10.1021/acs.analchem.0c05069>.
30. Crittenden CM, Akin LD, Morrison LJ, Trent MS, Brodbelt JS. 2017. Characterization of lipid A variants by energy-resolved mass spectrometry: impact of acyl chains. *J Am Soc Mass Spectrom* 28:1118–1126. <https://doi.org/10.1007/s13361-016-1542-6>.
31. Hankins JV, Madsen JA, Needham BD, Brodbelt JS, Trent MS. 2013. The outer membrane of Gram-negative bacteria: lipid A isolation and characterization. *Methods Mol Biol* 966:239–258. [https://doi.org/10.1007/978-1-62703-245-2\\_15](https://doi.org/10.1007/978-1-62703-245-2_15).
32. Henderson JC, O'Brien JP, Brodbelt JS, Trent MS. 2013. Isolation and chemical characterization of lipid A from gram-negative bacteria. *J Vis Exp* 2013:50623. <https://doi.org/10.3791/50623>.
33. Lakkaraju SK, Yu W, Raman EP, Hershfeld AV, Fang L, Deshpande DA, MacKerell AD, Jr. 2015. Mapping functional group free energy patterns at protein occluded sites: nuclear receptors and G-protein coupled receptors. *J Chem Inf Model* 55:700–708. <https://doi.org/10.1021/ci500729k>.
34. Raman EP, Yu W, Lakkaraju SK, MacKerell AD, Jr. 2013. Inclusion of multiple fragment types in the site identification by ligand competitive saturation (SILCS) approach. *J Chem Inf Model* 53:3384–3398. <https://doi.org/10.1021/ci4005628>.
35. Yu W, Lakkaraju SK, Raman EP, Fang L, MacKerell AD, Jr. 2015. Pharmacophore modeling using site-identification by ligand competitive saturation (SILCS) with multiple probe molecules. *J Chem Inf Model* 55:407–420. <https://doi.org/10.1021/ci500691p>.
36. van Eden W, Spiering R, Broere F, van der Zee R. 2012. A case of mistaken identity: HSPs are not DAMPs but DAMPERs. *Cell Stress Chaperones* 17:281–292. <https://doi.org/10.1007/s12192-011-0311-5>.
37. Chakafana G, Shonhai A. 2021. The role of non-canonical Hsp70s (Hsp110/Grp170) in cancer. *Cells* 10:254. <https://doi.org/10.3390/cells10020254>.
38. Murshid A, Borges TJ, Bonorino C, Lang BJ, Calderwood SK. 2019. Immunological outcomes mediated upon binding of heat shock proteins to scavenger receptors SCARF1 and LOX-1, and endocytosis by mononuclear phagocytes. *Front Immunol* 10:3035. <https://doi.org/10.3389/fimmu.2019.03035>.
39. Santos TG, Martins VR, Hajj GNM. 2017. Unconventional secretion of heat shock proteins in cancer. *Int J Mol Sci* 18:946. <https://doi.org/10.3390/ijms18050946>.
40. Zani IA, Stephen SL, Mughal NA, Russell D, Homer-Vanniasinkam S, Wheatcroft SB, Ponnambalam S. 2015. Scavenger receptor structure and function in health and disease. *Cells* 4:178–201. <https://doi.org/10.3390/cells4020178>.
41. Lokhande AS, Jahagirdar P, Dandekar P, Devarajan PV. 2019. Scavenger receptor and targeting strategies, p 297–321. *In* Devarajan P, Dandekar P, D'Souza A. (ed), Targeted intracellular drug delivery by receptor mediated endocytosis, vol 39. Springer International Publishing, Berlin, Germany.
42. Johnson BJ, Le TTT, Dobbin CA, Banovic T, Howard CB, Flores F, d M L, Vanags D, Naylor DJ, Hill GR, Suhrbier A. 2005. Heat shock protein 10 inhibits lipopolysaccharide-induced inflammatory mediator production. *J Biol Chem* 280:4037–4047. <https://doi.org/10.1074/jbc.M411569200>.
43. Bossaller L, Chiang PI, Schmidt-Lauber C, Ganesan S, Kaiser WJ, Rathinam VA, Mocarski ES, Subramanian D, Green DR, Silverman N, Fitzgerald KA, Marshak-Rothstein A, Latz E. 2012. Cutting edge: FAS (CD95) mediates noncanonical IL-1 $\beta$  and IL-18 maturation via caspase-8 in an RIP3-independent manner. *J Immunol* 189:5508–5512. <https://doi.org/10.4049/jimmunol.1202121>.
44. Shenderov K, Riteau N, Yip R, Mayer-Barber KD, Oland S, Hieny S, Fitzgerald P, Oberst A, Dillon CP, Green DR, Cerundolo V, Sher A. 2014. Cutting edge: endoplasmic reticulum stress licenses macrophages to produce mature IL-1 $\beta$  in response to TLR4 stimulation through a caspase-

- 8- and TRIF-dependent pathway. *J Immunol* 192:2029–2033. <https://doi.org/10.4049/jimmunol.1302549>.
45. Newton K, Wickliffe KE, Maltzman A, Dugger DL, Reja R, Zhang Y, Roose-Girma M, Modrusan Z, Sagolla MS, Webster JD, Dixit VM. 2019. Activity of caspase-8 determines plasticity between cell death pathways. *Nature* 575:679–682. <https://doi.org/10.1038/s41586-019-1752-8>.
  46. Pessoa CC, Reis LC, Ramos-Sanchez EM, Orikaza CM, Cortez C, de Castro Levatti EV, Badaro ACB, Yamamoto J, D'Almeida V, Goto H, Mortara RA, Real F. 2019. ATP6V0d2 controls Leishmania parasitophorous vacuole biogenesis via cholesterol homeostasis. *PLoS Pathog* 15:e1007834. <https://doi.org/10.1371/journal.ppat.1007834>.
  47. Xia Y, Liu N, Xie X, Bi G, Ba H, Li L, Zhang J, Deng X, Yao Y, Tang Z, Yin B, Wang J, Jiang K, Li Z, Choi Y, Gong F, Cheng X, O'Shea JJ, Chae JJ, Laurence A, Yang XP. 2019. The macrophage-specific V-ATPase subunit ATP6V0D2 restricts inflammasome activation and bacterial infection by facilitating autophagosome-lysosome fusion. *Autophagy* 15:960–975. <https://doi.org/10.1080/15548627.2019.1569916>.
  48. Wang G, Wang Q, Fan Y, He X. 2017. Reticulocalbin 2 correlates with recurrence and prognosis in colorectal cancer. *Am J Cancer Res* 7:2169–2179.
  49. Chang Z, Yan G, Yan H, Zheng J, Liu Z. 2019. Reticulocalbin 2 enhances osteogenic differentiation of human vascular smooth muscle cells in diabetic conditions. *Life Sci* 233:116746. <https://doi.org/10.1016/j.lfs.2019.116746>.
  50. Singh P, Dejager L, Amand M, Theatre E, Vandereyken M, Zurashvili T, Singh M, Mack M, Timmermans S, Musumeci L, Dejardin E, Mustelin T, Van Ginderachter JA, Moutschen M, Oury C, Libert C, Rahmouni S. 2015. DUSP3 genetic deletion confers M2-like macrophage-dependent tolerance to septic shock. *J Immunol* 194:4951–4962. <https://doi.org/10.4049/jimmunol.1402431>.
  51. Ondee T, Gillen J, Visitchanakun P, Somparn P, Issara-Amphorn J, Dang Phi C, Chancharoentana W, Gurusamy D, Nita-Lazar A, Leelahavanichkul A. 2019. Lipocalin-2 (Lcn-2) attenuates polymicrobial sepsis with LPS pre-conditioning (LPS tolerance) in FcγRIIb deficient lupus mice. *Cells* 8:1064. <https://doi.org/10.3390/cells8091064>.
  52. Strand ME, Aronsen JM, Braathen B, Sjaastad I, Kvaloy H, Tonnessen T, Christensen G, Lunde IG. 2015. Shedding of syndecan-4 promotes immune cell recruitment and mitigates cardiac dysfunction after lipopolysaccharide challenge in mice. *J Mol Cell Cardiol* 88:133–144. <https://doi.org/10.1016/j.yjmcc.2015.10.003>.
  53. Phulphagar K, Kuhn LI, Ebner S, Frauenstein A, Swietlik JJ, Rieckmann J, Meissner F. 2021. Proteomics reveals distinct mechanisms regulating the release of cytokines and alarmins during pyroptosis. *Cell Rep* 34:108826. <https://doi.org/10.1016/j.celrep.2021.108826>.
  54. Barker JH, Weiss JP. 2019. Detecting lipopolysaccharide in the cytosol of mammalian cells: Lessons from MD-2/TLR4. *J Leukoc Biol* 106:127–132. <https://doi.org/10.1002/JLB.3MIR1118-434R>.
  55. Rathinam VAK, Zhao Y, Shao F. 2019. Innate immunity to intracellular LPS. *Nat Immunol* 20:527–533. <https://doi.org/10.1038/s41590-019-0368-3>.
  56. Lorey MB, Rossi K, Eklund KK, Nyman TA, Matikainen S. 2017. Global characterization of protein secretion from human macrophages following non-canonical caspase-4/5 inflammasome activation. *Mol Cell Proteomics* 16:S187–S199. <https://doi.org/10.1074/mcp.M116.064840>.
  57. Fang H, Liu A, Sun J, Kitz A, Dirsch O, Dahmen U. 2013. Granulocyte colony stimulating factor induces lipopolysaccharide (LPS) sensitization via upregulation of LPS binding protein in rat. *PLoS One* 8:e56654. <https://doi.org/10.1371/journal.pone.0056654>.
  58. Conus S, Simon HU. 2010. Cathepsins and their involvement in immune responses. *Swiss Med Wkly* 140:w13042. <https://doi.org/10.4414/smw.2010.13042>.
  59. Hao L, Zhu G, Lu Y, Wang M, Jules J, Zhou X, Chen W. 2015. Deficiency of cathepsin K prevents inflammation and bone erosion in rheumatoid arthritis and periodontitis and reveals its shared osteoimmune role. *FEBS Lett* 589:1331–1339. <https://doi.org/10.1016/j.febslet.2015.04.008>.
  60. Zhu W, Li J, Liu Y, Xie K, Wang L, Fang J. 2016. Mesencephalic astrocyte-derived neurotrophic factor attenuates inflammatory responses in lipopolysaccharide-induced neural stem cells by regulating NF-κB and phosphorylation of p38-MAPKs pathways. *Immunopharmacol Immunotoxicol* 38:205–213. <https://doi.org/10.3109/08923973.2016.1168433>.
  61. Gottschalk RA, Martins AJ, Angermann BR, Dutta B, Ng CE, Uderhardt S, Tsang JS, Fraser ID, Meier-Schellersheim M, Germain RN. 2016. Distinct NF-κB and MAPK activation thresholds uncouple steady-state microbe sensing from anti-pathogen inflammatory responses. *Cell Syst* 2:378–390. <https://doi.org/10.1016/j.cels.2016.04.016>.
  62. Joshi VD, Kalvakolanu DV, Hasday JD, Hebel RJ, Cross AS. 2002. IL-18 levels and the outcome of innate immune response to lipopolysaccharide: importance of a positive feedback loop with caspase-1 in IL-18 expression. *J Immunol* 169:2536–2544. <https://doi.org/10.4049/jimmunol.169.5.2536>.
  63. Joshi VD, Kalvakolanu DV, Hebel JR, Hasday JD, Cross AS. 2002. Role of caspase 1 in murine antibacterial host defenses and lethal endotoxemia. *Infect Immun* 70:6896–6903. <https://doi.org/10.1128/IAI.70.12.6896-6903.2002>.
  64. Gottschalk RA, Dorrington MG, Dutta B, Krauss KS, Martins AJ, Uderhardt S, Chan W, Tsang JS, Torabi-Parizi P, Fraser ID, Germain RN. 2019. IFN-mediated negative feedback supports bacteria class-specific macrophage inflammatory responses. *Elife* 8:e46836. <https://doi.org/10.7554/eLife.46836>.
  65. Strohal M, Kavan D, Novak P, Volny M, Havlicek V. 2010. mMass 3: a cross-platform software environment for precise analysis of mass spectrometric data. *Anal Chem* 82:4648–4651. <https://doi.org/10.1021/ac100818g>.
  66. Ong SE, Blagoev B, Kratchmarova I, Kristensen DB, Steen H, Pandey A, Mann M. 2002. Stable isotope labeling by amino acids in cell culture, SILAC, as a simple and accurate approach to expression proteomics. *Mol Cell Proteomics* 1:376–386. <https://doi.org/10.1074/mcp.m200025-mcp200>.
  67. Rayamajhi M, Zhang Y, Miao EA. 2013. Detection of pyroptosis by measuring released lactate dehydrogenase activity. *Methods Mol Biol* 1040:85–90. [https://doi.org/10.1007/978-1-62703-523-1\\_7](https://doi.org/10.1007/978-1-62703-523-1_7).
  68. Shevchenko A, Tomas H, Havlis J, Olsen JV, Mann M. 2006. In-gel digestion for mass spectrometric characterization of proteins and proteomes. *Nat Protoc* 1:2856–2860. <https://doi.org/10.1038/nprot.2006.468>.
  69. Cox J, Mann M. 2008. MaxQuant enables high peptide identification rates, individualized p.p.b.-range mass accuracies and proteome-wide protein quantification. *Nat Biotechnol* 26:1367–1372. <https://doi.org/10.1038/nbt.1511>.
  70. Cox J, Neuhauser N, Michalski A, Scheltema RA, Olsen JV, Mann M. 2011. Andromeda: a peptide search engine integrated into the MaxQuant environment. *J Proteome Res* 10:1794–1805. <https://doi.org/10.1021/pr101065j>.
  71. Tyanova S, Temu T, Sinitcyn P, Carlson A, Hein MY, Geiger T, Mann M, Cox J. 2016. The Perseus computational platform for comprehensive analysis of (prote)omics data. *Nat Methods* 13:731–740. <https://doi.org/10.1038/nmeth.3901>.
  72. Sturn A, Quackenbush J, Trajanoski Z. 2002. Genesis: cluster analysis of microarray data. *Bioinformatics* 18:207–208. <https://doi.org/10.1093/bioinformatics/18.1.207>.
  73. Mi H, Muruganujan A, Huang X, Ebert D, Mills C, Guo X, Thomas PD. 2019. Protocol update for large-scale genome and gene function analysis with the PANTHER classification system (v.14.0). *Nat Protoc* 14:703–721. <https://doi.org/10.1038/s41596-019-0128-8>.
  74. Petersen TN, Brunak S, von Heijne G, Nielsen H. 2011. SignalP 4.0: discriminating signal peptides from transmembrane regions. *Nat Methods* 8:785–786. <https://doi.org/10.1038/nmeth.1701>.
  75. Bendtsen JD, Jensen LJ, Blom N, Von Heijne G, Brunak S. 2004. Feature-based prediction of non-classical and leaderless protein secretion. *Protein Eng Des Sel* 17:349–356. <https://doi.org/10.1093/protein/gzh037>.
  76. Almagro Armenteros J, Tsirigos KD, Sonderby CK, Petersen TN, Winther O, Brunak S, von Heijne G, Nielsen H. 2019. SignalP 5.0 improves signal peptide predictions using deep neural networks. *Nat Biotechnol* 37:420–423. <https://doi.org/10.1038/s41587-019-0036-z>.
  77. Kim HM, Park BS, Kim JI, Kim SE, Lee J, Oh SC, Enkhbayar P, Matsushima N, Lee H, Yoo OJ, Lee JO. 2007. Crystal structure of the TLR4-MD-2 complex with bound endotoxin antagonist eritoran. *Cell* 130:906–917. <https://doi.org/10.1016/j.cell.2007.08.002>.
  78. Ustach VD, Lakkaraju SK, Jo S, Yu W, Jiang W, MacKerell AD, Jr. 2019. Optimization and evaluation of site-identification by ligand competitive saturation (SILCS) as a tool for target-based ligand optimization. *J Chem Inf Model* 59:3018–3035. <https://doi.org/10.1021/acs.jcim.9b00210>.
  79. Perez-Riverol Y, Csordas A, Bai J, Bernal-Llinares M, Hewapathirana S, Kundu DJ, Inuganti A, Griss J, Mayer G, Eisenacher M, Perez E, Uszkoreit J, Pfeuffer J, Sachsenberg T, Yilmaz S, Tiwary S, Cox J, Audain E, Walzer M, Jarnuczak AF, Ternent T, Brazma A, Vizcaino JA. 2019. The PRIDE database and related tools and resources in 2019: improving support for quantification data. *Nucleic Acids Res* 47:D442–D450. <https://doi.org/10.1093/nar/gky1106>.